A Medium-Voltage Magnetic Component Testing System

10th semester project

Master's Thesis

WRITTEN BY:
FREDERIK HJORTKÆR PETERSEN
HIJAB CHAUDHARY

M4
GROUP PED4 - 1043
DEPARTMENT OF ENERGY TECHNOLOGY
AALBORG UNIVERSITY

AALBORG UNIVERSITY
STUDENT REPORT

School of Engineering and Science (SES)
Energy Engineering
Pontoppidanstræde 111
9220 Aalborg Ø, Denmark
http://www.ses.aau.dk/

Title:
A Medium-Voltage Magnetic Component Testing System

10th Semester Project

Master's Thesis

Project period:

February 2021 - May 2021

Project group:

PED4 - 1043

Participants:

Frederik Hjortkær Petersen

Frederik Hjortkær Petersen

Hijab

Hijab Chaudhary

Supervisors:
Huai Wang
Zhan Shen

Circulation: Uploaded digitally
Page count: 51
Appendix count: 0
Appendix pages: 0
Finished: May 27, 2021

Abstract:

Transformers are one of the most widely used electrical equipment in power distribution and electronics systems. As these applications require the components to fulfil the system operating conditions, the transformer needs to be tested. This report focuses on a testing system that emulates real-life conditions for high-frequency transformers. Different topologies are described, and an extended Dual-Active Bridge (DAB) has been chosen for implementing the testing system. To drive the DAB, different switching topologies are investigated. The simulations and experiments are performed with a single phase-shift between the primary and secondary converter's gating signals. In the extended DAB, the power circulates between the primary and the secondary to minimize the power required from the power supply. The effect on the circulating path is investigated. The system is modelled and simulated in PLECS Standalone. In the system, the controllable parameters are the switching frequency, the phase-shift and the duty cycle. The influence of these parameters to the transformer conditions are investigated by open-loop simulations. Then, closed-loop control of the phase-shift is derived to control the transformer current. The control is applied to the simulations and the experimental setup. The system is constructed in the laboratory and controlled using a PLECS RT box 1 and PLECS Coder. Based on the simulation results of the closed-loop controller, a conclusion is made of the testing system performance.

By signing this document, each member of the group confirms participation on equal terms in the process of writing the project. Thus, each member of the group is responsible for the all contents in the project.

Summary

This report focuses on the design of the medium-voltage magnetic component testing system, being capable of emulating realistic operating conditions of the high-frequency transformers. The design to fulfil a specific voltage, current and frequency range of the testing system. In Chapter 1, the basic background of the topic is provided, including the existing magnetic component testing systems, their limitations, as well as the specifications of the realistic magnetic component testing system. Based on the literature study, different circuit topologies which have the potential to be used for this system are investigated. Additionally, the research question is formulated along with the main objectives and the project limitations based on the project scope.

In Chapter 2, the chosen extended Dual-Active Bridge (DAB) topology is defined and discussed. At first, different control methods for the topology are discussed with their performance details. Based on that, Single Phase-Shift (SPS) control system is found to be more accurate and therefore selected as the operational principle of the project. Moreover, it is discussed in detail the different switching combinations. It plays a vital role in the project operation by saving energy significantly in the long term testing.

Chapter 3 illustrates the open-loop based simulation testing of a high-frequency transformer. The details of the simulation circuit are provided. Suitable system parameters that are used are stated. The system is tested for different switching frequencies, and the tested results are described along with the performance analysis. To further test the system, the analysis is done by varying the phase shift to different values. For further testing of accuracy, tests for the different duty cycles are conducted as well, and their results are shown at the end of the chapter.

To enhance the system performance, in Chapter 4, a closed-loop phase-shift controller is designed to control the primary current. First, the modelling of the closed-loop controller is described and discussed. Afterwards, the controller design is performed. The system is simulated for performance analysis, and the results of the simulated closed-loop controller are presented. To test the controller performance, the current reference has been changed from a single step to several steps. This test is conducted with different switching frequency values.

In chapter 5, the hardware and experimental analysis are illustrated. The hardware of the circuit is managed to be built. Furthermore, the interface between the software developed model and hardware setup is completed and made functional. However, due to the COVID-19 pandemic and subsequent lock-down of the university, the laboratory was not accessible most of the time during this semester. Thus, the experimental testing of the setup and the phase-shift controller are aimed to be performed as future works.

Chapter 6 concludes the report on achieving the objectives stemming from the research question presented in Section 1.4. The realistic magnetic components testing system is therefore designed with the desired performances. Finally, further work that can be possibly done relevant to this project is presented in Chapter 7.

Preface

This report is written by group *PED4-1043* from the Department of Energy Technology at Aalborg University, which consists of two students on the fourth semester of the Master study. The theme of this 4^{th} semester Master project is *Master's Thesis*.

In order to complete the semester project, the software used are listed below.

- **Overleaf** - Report writing.
- **MATLAB & Simulink** - Modelling, calculations and control of the system.
- **PLECS Standalone** - System modelling and simulations.
- **PLECS Coder** - Configure PLECS RT box 1 to setup.
- **Draw i/o** - Drawing and editing figures.

Reader's Guide:

Sources will be cited using the Vancouver Method, [number, page]. The number represents which source in the bibliography that is cited. Books in the bibliography are denoted 'author, title, publisher, edition, year of publication', while web pages are denoted 'author, title, URL, year of publication. Also if a reference is placed at the end of a section, the whole section is related to that reference.

Equations will be referred with an equation number, which is listed on the right hand side of the corresponding equation. These equations numbers are denoted by the which number of equation in a given chapter it is. As an example, equation number 2 in chapter 4 will be referenced as 'Eq. 4.2'.

Figures and Tables will be referenced by the number of which it is in a given chapter, similar to how the equation number is derived. The Figure number and caption will appear below the corresponding Figure, while the Table number and caption will appear above the given Table.

Table of Contents

Nomenclature

Acronyms

DAB Dual-Active Bridge

DPS Dual Phase-Shift

DUT Device Under Testing

EMI Electro-Magnetic Interference

EPS Extended Phase-Shift

FPGA Field-Programmable Gate Array

HIL Hardware-in-the-loop

MFT Medium Frequency Transformer

MOSFET Metal-Oxide-Semiconductor Field-Effect Transistors

PCB Printed Circuit Board

PI Propotional-Integral

PWM Pulse Width Modulation

RMS Root-Mean-Square

SPS Single Phase-Shift

SS Steady-State

TPS Triple Phase-Shift

ZOH Zero Order Hold

ZVS Zero-Voltage-Switching

FEM Finite-Element-Method

Variables

Symbol	Description	Unit
C_1	Input smoothing capacitor	$[F]$
C_2	Output smoothing capacitor	$[F]$
C_b	Blocking capacitor	$[F]$
C_D	Continuous transfer function for the phase-shift PI controller	$[-]$
$C_{D,fsw}$	Continuous transfer function for the f_{sw} tuned C_D	$[-]$
C_r	Resonance capacitor	$[F]$
D	Phase-shift angle	$[^o]$
f_{sw}	Switching frequency	$[Hz]$
i_{ac}	AC current	$[A]$
i_{circ}	Circulating current	$[A]$
I_{dc}	DC source current	$[A]$

Symbol	Description	Unit
I_{error}	Current error for the phase-shift control	$[A]$
$I_{p,rms}$	RMS primary current	$[A]$
I_{ref}	Current reference for the Phase-shift control	$[A]$
K	Factor for the gate signal generator	$[-]$
K_i	Integral gain	$[-]$
$K_{i,fsw}$	Switching frequency dependant integral gain	$[-]$
K_p	Proportional gain	$[-]$
$K_{p,fsw}$	Switching frequency dependant proportional gain	$[-]$
L_{co}	Control inductor	$[H]$
L_{lk}	Leakage inductor	$[H]$
R_c	Series resistor with smoothing capacitor	$[\Omega]$
R_{co}	Control resistor	$[\Omega]$
R_d	Dissipation resistor	$[\Omega]$
R_{in}	Input source resistor	$[\Omega]$
R_{lk}	Leakage resistor	$[\Omega]$
S	Switch gating signal	$[-]$
U_{ac1}	Primary AC voltage	$[V]$
U_{ac2}	Secondary AC voltage	$[V]$
U_{dc1}	Input DC voltage	$[V]$
U_{dc2}	Output DC voltage	$[V]$
δ	Duty cycle	$[-]$

Chapter 1

Introduction

Magnetic components, e.g. transformers, are considered as one of the most widely used electrical components in power distribution and electronics systems. Due to the rapid growth of the social economy, the inclination in the power grid-scale is observed. Traditional power transformers are excessively used to step up/step down of voltages and currents, power transfer, isolation between the circuits, decoupling of noise and phase shifting, etc. [1]. Although such transformers are efficient and reliable, they have some limitations too [2]. Conventional power transformers are larger in size, higher in cost, unable to detect the short circuit faults and they are inefficient in isolating the harmonics components etc. Power electronics/high-frequency transformers, on the other hand, are designed with improved features in order to cope with the shortcomings of the traditional power transformers.

Power electronics transformers, also known as solid-state transformers, are widely used in several power electronics applications. Solid-state transformers mainly use multi-stage power electronics converters. In such converters, a medium-frequency or high-frequency transformer is usually used for galvanic isolation. They are becoming more and more popular due to the high power densities, and high blocking capabilities [3]. With the increasing research and the use of the power system applications in traction, these transformers are highly demanded for the galvanic isolation. Also, the magnetic materials in them are designed to be more efficient in operation as well as produce less losses [3]. Moreover, by increasing the operating frequency of the power transformers, the size of the transformer is reduced. It also makes the system compact and cost-effective. Therefore, power electronics transformers with reduced sizes and cost are the most desirable. These transformers require reliability testing under high-frequency stress. Realistic characterizations and insulation capability testing of these transformers are also necessary for optimal sizing for the applications.

Magnetic component testing systems plays a vital role in order to determine the overall efficiency, which is the most desirable goal in the power electronics systems. It is used to obtain the magnetic properties of the transformer. Also, it determines the parasitic capacitance in the system that can be reduced in order to avoid the Electro-Magnetic Interference (EMI) effect produced during the operation [4]. These parasitic elements cause unwanted behaviour or power loss in the system.

1.1 Limitations in existing Testing Systems

There are some existing magnetic component testing systems that are used to test the power transformers. However, these testing systems have some limitations.

Impedance analyser and B-H analysers, for example, are used to test the magnetic component systems with high-frequency range. But, these testing systems are not capable of operating for the high voltage and are limited up to 400V [5]. This is the main drawback of them. Although they are efficient in working for the high-frequency range, they are unable to characterise the high voltage transformers at the high excitation level that are required in the power electronics applications.

In the medium/high voltage transformers, insulation testing is essential. There are some existing insulation testing systems for the transformers as well. However, the relevant standards of them are mainly limited to the line frequency transformers. The insulation frequency of these systems is limited to 50/60 [Hz]. Therefore, such testing systems are not feasible for the high-frequency range transformers testing.

There are no commercial testing systems available that are capable of testing at the realistic operating conditions and can be used to emulate the behaviour of high-frequency and voltage transformer. It is therefore very useful to investigate a magnetic component testing system that is capable of working at the medium to high voltage and frequency range.

1.2 Realistic Magnetic Component Testing System

For the designing of the medium/high voltage and frequency magnetic component testing system, there are key aspects that need to be considered. Some of these key aspects are listed below.

- The testing system should have the capability to emulate the operation conditions of the transformers to be tested. In this way, the control methods can be used to generate the required voltage and current waveform.
- For the testing system, a power supply is required as well. The purpose is to limit the power needed from the power supply. An energy circulation scheme within the testing system is preferred. The power supply provides only the power losses of the testing system and the transformer samples under test.
- For the practical application, another consideration is to introduce the protection and the safety features for the operations above kV.

Regarding the first two aspects of considerations, proper circuit topology and control scheme need to be used. Especially, an energy recycling scheme is necessary to limit the required power supply for the power loss of the testing system only.

1.3 Circuit Topologies

A back-to-back topology structure is a reasonable choice for designing the magnetic component testing system as it has the ability to recycle the power and provide a voltage path in the system. There are different back to back topology structures. Based on the literature study, two of them are discussed in the sections below.

1.3.1 Back-to-Back Resonant Topology

In [6], the back-to-back resonant testing topology is presented and discussed. The basic structure of this topology is shown in Fig. 1.1. It consists of a Medium Frequency Transformer (MFT) with a primary side connected to the actively switched H-bridge and the secondary side connected to the diode H-bridge rectifier. The diode rectifier is further connected to the DC bus capacitors. Besides, in order to generate the resonance, two distributed resonance capacitors C_{r1} and C_{r2} are connected between the two sides of the MFT. The switching frequency and the duty cycle is kept constant, and the setup will operate as a resonant converter.

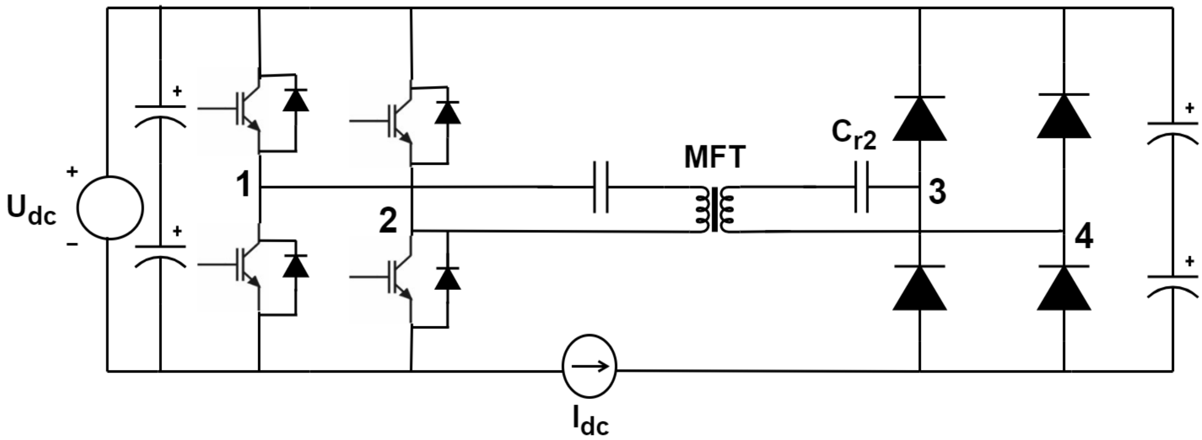

Figure 1.1: Back to Back Resonant Active Topology [6]

It can be seen in Fig. 1.1 that the positive and negative bus of both sides of the MFT are interconnected with each other. For the control of power flow, the negative bus is interconnected through the dc current source I_{dc}. The reason is that on the secondary side, diodes are present, which are unidirectional. These diodes are unable to redirect the current in the opposite direction. With the help of this I_{dc} the current is controlled in both directions. By setting the required parameters of the resonant capacitors and maintaining the switching frequency constant, the resonant converter operation can be achieved.

The main disadvantage of this topology is the large amount of dc current source I_{dc} in the circuit. To realise such a large current, instruments are required as well, which causes complexity in the system. It also increases the overall cost of the system. So practically, it is not very desirable to have this current source in the circuit. Therefore an alternate will need to be applied. One candidate is an extension of the standard Dual-Active Bridge.

1.3.2 Dual Active Bridge Topology

The DAB is considered as an ideal topology due to its several advantages over other topologies e.g. energy recycle, galvanic isolation capability, higher efficiency and high power density [7]. The extended topology of DAB is presented in Fig. 1.2. In the conventional DAB, the circulating current path is not connected, and it is not used for recycling the power. Utilising this extended structure enables current recovering and testing of the transformer in a wide frequency range as it can be controlled with a specified switching frequency. The gating signals for the power electronic components, which in Fig. 1.2 are Metal-Oxide-Semiconductor Field-Effect Transistors (MOSFET), is generated using Pulse Width Modulation (PWM).

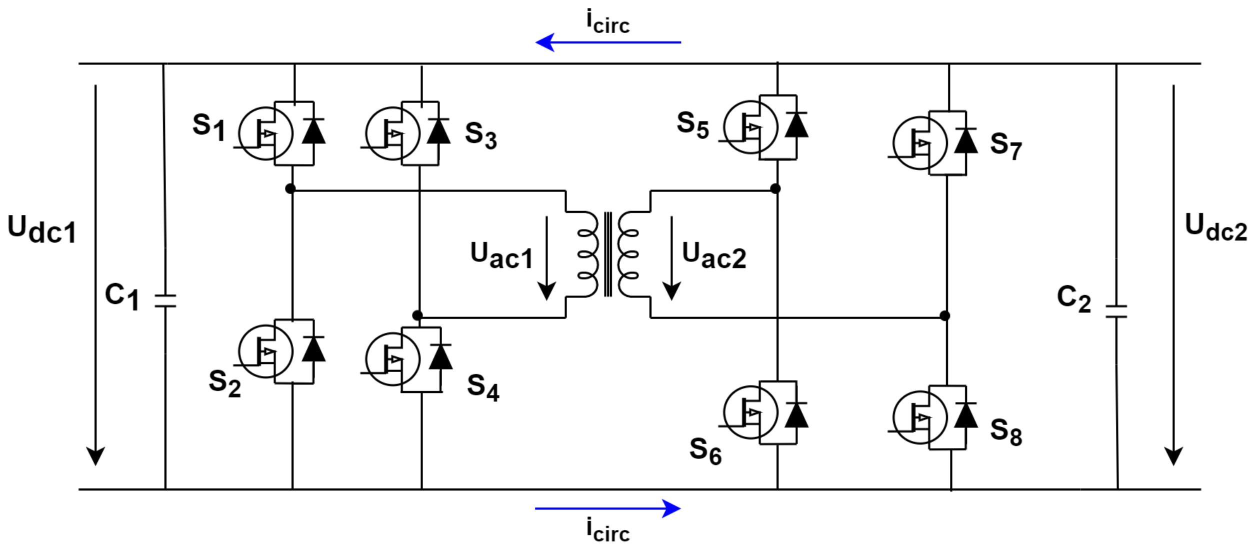

Figure 1.2: Extended Dual Active Bridge topology [3]

It consists of two 4-switch converters connected to the primary and the secondary sides of the transformer. C_1 and C_2 are the smoothing capacitors for both ends. U_{dc1} and U_{dc2} are the DC voltages at both ends. Both primary and secondary bridges are kept operating with a 50% duty cycle in order to balance the transformer. By utilizing the circulating current path, the energy can be transferred in both directions.

In order to control the power flow, a phase shift is introduced between the gating signals of the two converters. Thereby a phase shift occurs between the AC voltages generated by the two bridges. If the AC voltages at the primary and the secondary side are the same, there will be no power flow. If some phase difference is introduced in the AC voltages, the AC current starts to flow in the secondary circuit [3]. The value of this AC current I_{ac} depends on the phase shift as well as the parasitics in the transformer. [3]

Generally, the winding resistance is much smaller than the leakage inductance, and the magnetisation inductance is much larger value. The DAB topology circuit is simplified as represented in Fig. 1.3 [3].

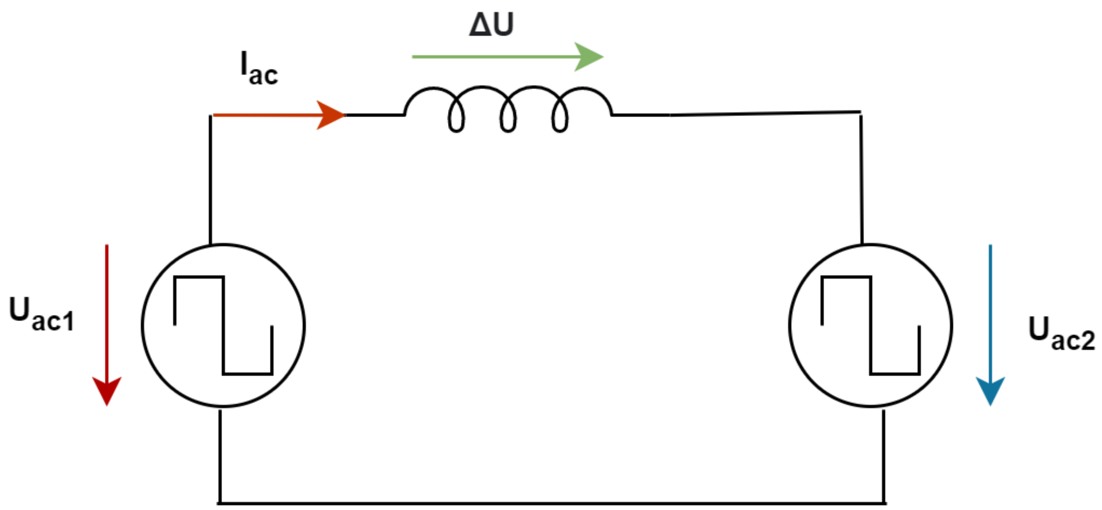

Figure 1.3: DAB Equivalent Circuit [3]

In Fig. 1.3, both of the converters can generate positive, negative and zero volts square wave voltages. The detailed DAB operational principles are discussed in the following chapters.

Unlike the back-to-back resonant topology, DAB does not require a large DC current source for the control of the power flow while having the same input dc voltage source. Also, back-to-back resonant topology using diodes provides less control flexibility while having the same amount of components as DAB. Therefore, DAB is preferred for the testing system. A modified DAB topology is considered more feasible, and it is used for further investigation in this project.

1.4 Research Question

Based on the given analysis above, the following research question is proposed.

"How can the efficient magnetic component testing system be designed that is capable of emulating more realistic operating conditions of the high-frequency transformer?"

This research question will serve as a major part of the report. By considering the outcomes of the previously conducted research as well and the limitations of them, an investigation for the ideal magnetic component testing system will be processed.

1.5 Project Objectives

This project aims to fulfil the following objectives in order to achieve the desired goals.

- Define the suitable requirements of the magnetic component testing system that is designed to operate at realistic operating conditions. With the help of a literature study, investigate the topology that could possibly be used in order to fulfil the requirements of the testing system.
- As per desired requirements, develop the model of the magnetic component testing system. Also, for the model, consider the parasitic elements that are present during the practical operation.
- Simulate the developed model. Analyse the results of the simulated model in order to validate the performance of the system.
- Formulate improvement to the system in order to enhance the performance of the testing system.

Besides, another main objective of this project is to design a system within the specific voltage, current and frequency range. This is required to accomplish the technical requirements of the designed testing system. These technical specifications are presented in the Table 1.1.

Table 1.1: Testing system requirements

System	Description	Maximum	Tolerance
Current	Input current	2 [A]	±0.1 [A]
	Transformer AC peak current	20 [A]	±0.1 [A]
	Circulating path	20 [A]	±0.1 [A]
Voltage	Input voltage	2000 [V]	-
	Output Voltage	2000 [V]	±3% [V]
Frequency	Switching frequency	250 [kHz]	-
Efficiency	Transformer	100%	−10%

In addition to the project requirements, the project is also subjected to some limitations. These limitations are presented in the following section.

1.6 Project Limitations

During the process of this project, there are some limitations that influenced the progress. These limitations occurred due to COVID-19 and its government imposed restrictions subjected to Aalborg University. The limitations affecting this project is described in the following:

- The laboratory is closed for the most part of the project period due to COVID-19 restrictions. Access to the laboratory is given in the latter part of the project period and thereby limiting the amount of experimental work.
- In the laboratory, for the experimental testing, it is not possible to supply the system with the required voltage level presented in Table 1.1. Therefore, only the software simulation testings use the required voltage for the DC source.
- As mentioned in section 1.2, the protection and safety features are relevant to be introduced for realistic magnetic component system operations. However, due to the above mentioned laboratory access restrictions, the implementation of them is not possible in the given time frame.

Chapter 2

Topology for the Magnetic Component Testing Setup - Dual Active Bridge

The main objective of the report is to utilise the DAB circuit in order to emulate the working conditions of a high-frequency transformer. In Chapter. 1, an extended version of the standard DAB circuit is introduced, where a circulating current path is added. Therefore the DAB circuit will be looked into before the simulation testing of the DAB system. In this Chapter, different kinds of operation principles to control the DAB system are introduced. Thereafter, an analysis of the circulating current path is given.

2.1 Operation principles

The different working principles for the DAB are studied in different literatures. In [8], an overview of four different control methods for the DAB circuit are discussed, namely SPS, Dual Phase-Shift (DPS), Extended Phase-Shift (EPS) and Triple Phase-Shift (TPS). They are introduced in the following.

2.1.1 Single Phase-Shift

The most common control method for the DAB is the SPS control. For this control method, the gating signals for the eight switches in Fig. 1.2, S_1-S_8, are square-wave signals with a 50% duty cycle and no zero component. The cross-connected switch pairs in both 4-switch converters are switched sequentially in order to generate a phase-shifted voltage with a duty cycle of 50% across the transformer's primary and secondary sides. The only controllable parameter is the phase-shift angle D, which affect the voltage across the transformer leakage inductor. Utilizing SPS has several advantages, such as small inertia, high dynamic and easy realization of soft-switching control. However, the power flow's control depends on the leakage inductor, which results in increasing current if the voltage amplitude of the primary and secondary side of the transformer is mismatched. In addition, for the whole power range the DAB can not operate under Zero-Voltage-Switching (ZVS) in this situation and therefore the power loss increases and the efficiency decreases [8]-[9].

2.1.2 Extended Phase-Shift

In the EPS control, the cross-connected switch pairs are switched in sequence in one of the four-switch converters, while in the other, the switch pairs are switched with an inner phase-shift. Thereby, contrary to the SPS control, in the EPS control, the gating signal for one of the four-switch converter has a zero component while the other converter remains unchanged. Therefore the ac voltage of the first converter is a three-level wave while the other is a two-level square wave with a 50% duty cycle. With the additional phase-shift the EPS control is control using an "outer" and an "inner" phase-shift, denoted D_1 and D_2 respectively. The outer phase-shift controls the direction and magnitude of the power flow, while the inner phase-shift is utilized in order to decrease the circulating power and expand the operation range of the ZVS. Different studies of the EPS have been carried out, which showed that compared to the SPS control, the system efficiency is improved and the ZVS operating range is expanded. In addition, the current stress is reduced and the regulating flexibility is improved [10].

2.1.3 Dual Phase-Shift

The DPS control method is similar to the EPS control, however in the DPS control the cross-connected switches in both 4-switch converters are with an "inner" phase-shift. The inner phase shift for both 4-switch converters is the same for this control. Therefore ac voltage on both sides of the transformer has a 3-level waveform. By utilizing the DPS control, instead of SPS control, the current stress and steady-state current are decreased. In this control method, the efficiency of the system is increased, ZVS operation range is expanded, and output capacitance is reduced. Contrary to the EPS control, the operation states of the two 4-switch converters are unchanged if the power flow direction or voltage conversion changes. Therefore the DPS is deemed easier to be implemented, and the dynamic performance is improved. [11]

2.1.4 Triple Phase-Shift

The TPS control is similar to the DPS control as the cross-connected switch pairs in both four-switch converter are switched with an "inner" phase-shift. Contrary to the DPS control, the "inner" phase-shifts might differ from each other. Therefore the TPS control has three controllable parameters which are the three duty cycles D_1, D_2 and D_3. Different studies of this control have been performed, which mainly regarded the optimization operation field [12]. While the TPS control is derived later than the SPS, EPS and DPS controls, the other three can be regarded as special cases of the TPS control [8].

In [8], the different controls are applied to the DAB system, and the different signals obtained are illustrated. The gating signals for all eight power electronic devices of the DAB circuit, the ac voltage of the primary and secondary side of the transformer, and the inductor current are illustrated in Fig. 2.1 for the four different control methods. The number of different duty cycles needed for each control differs while the same notations are applied.

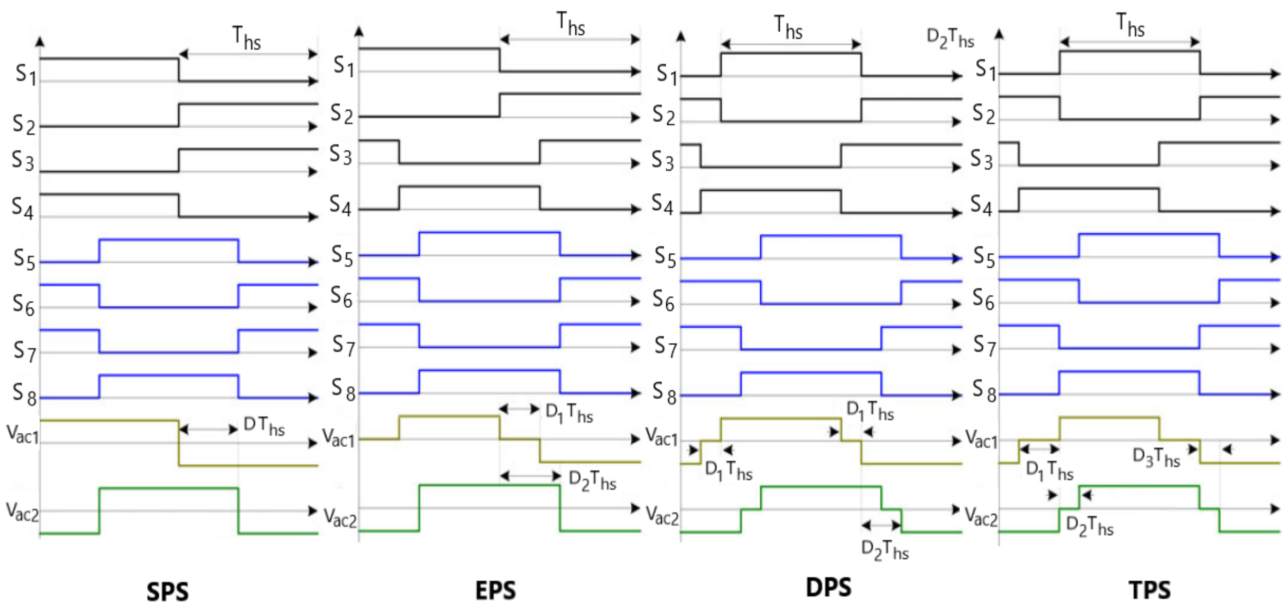

Figure 2.1: Gating signals, primary and secondary AC voltage and inductor current for the 4 switching topologies. [8]

In Fig. 2.1, it can be seen that each of the different controls has different gating signals for all eight switches. This results in different voltage waveforms for the primary and secondary of the transformer and the inductor current.

While each of these control methods can be applied, they each have their pros and cons. The SPS control is simple to realise. However, it has setbacks in regards to the ZVS range and the efficiency if certain system conditions are not met. While the EPS is an improvement to the SPS control, the operation states of the converters will need to be switched in order to attain a decreased circulating power. For the DPS control, the operation states do not need to be changed, compared to the EPS control. Therefore the DPS is a better choice compared to the EPS control. The TPS control is difficult to be implemented, but its controllability is higher than the other three. Since the TPS control have three controllable parameters, while the EPS and DPS have two and the SPS with one controllable parameter.

For the simplicity and discussed performance, either the SPS or the DPS control is applied for the simulation and experimental testing of the system. In addition, it is possible to make a comparative analysis of the effect of the four control methods on the testing if necessary.

2.2 Circulating current path

In the DAB circuit for this project, a circulating current path is added, which differs from the standard DAB structure. By utilizing this path, the power losses generated between the two 4-switch converters will primarily be taken into account by the input DC source. As the input and output DC voltages is set to the same reference, thereby the additional energy will flow through the circulating current path and supply the transformer current. In addition, the current flow can be uni-directional and bi-directional. The flow of the circulating current path current is illustrated in Fig. 2.2. Noted that the illustrated circulating current is defined as the positive current direction.

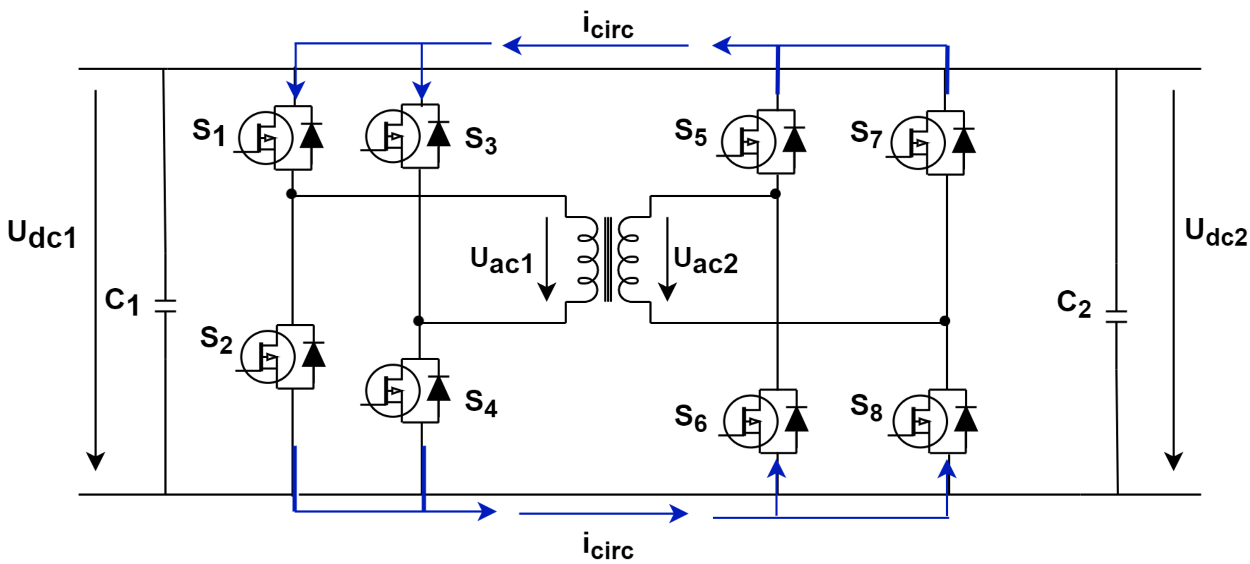

Figure 2.2: Circulating current path

Ideally, the circulating current will only flow through the converter branches and thereby, it will supplement the primary transformer current with the access energy from the secondary transformer current. Thereby the current supplied from the DC source is not required to be high. By initial simulation testing of the DAB system with the circulating current path, using the SPS control, it is discovered that there are two cases of the direction of the current flow. The circulating current direction are either positive, as illustrated in Fig. 2.2, or negative. In addition, it is discovered that within one switching period, there is a repeated cycle of four switching combinations in regards to the energy flow going through the circulating current path. Two of the switching combinations resulted in a positive circulating current flow, and the other two resulted in a negative current flow.

In Fig. 2.3 the circulating current, transformer AC voltage and the four gating signals are illustrated during one switching period in Steady-State (SS). The crossing switches in each converter are utilizing the same gating signal and therefore will only one of signals are shown. Also this is the case utilizing the system parameters given in Table 3.1 on page 14 in Chapter 3.

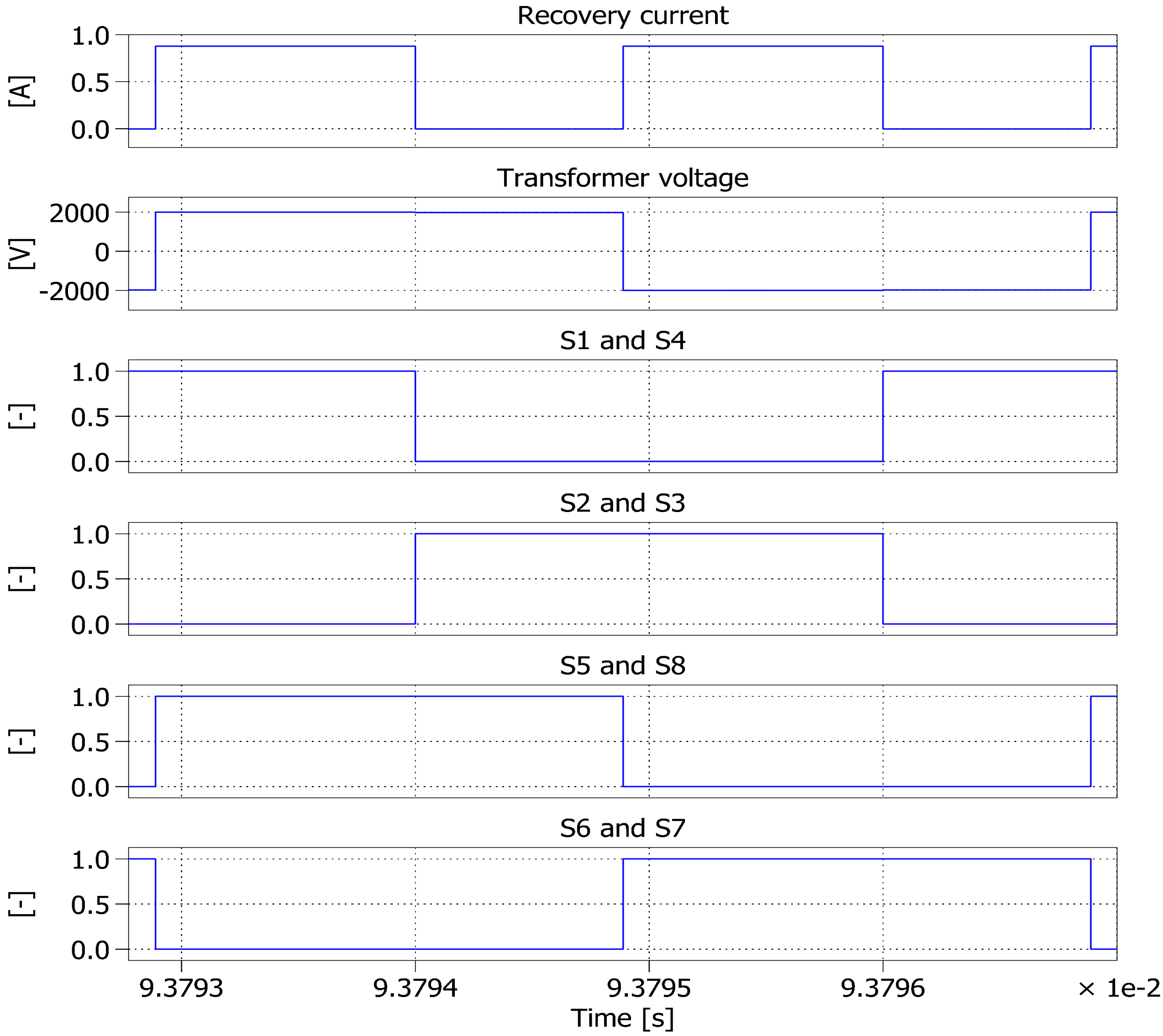

Figure 2.3: Circulating current and switching signals in one period (in SS)

As illustrated in 2.3, the circulating current is bi-directional. When a change occurs in the gating signals in either of the two 4-switch converters, a polarity change occurs in the circulating current. Thereby the frequency of the circulating current will be twice the switching frequency as shown in

Fig. 2.3. According to Fig. 2.3 the switching signal combinations resulting in a positive circulating current are when S1 and S4 and S5 and S8 are "ON", and when S2 and S3 and S6 and S7 are "ON". In addition, the negative circulating current occurs when S1 and S4 and S6 and S7 are "ON", and when S2 and S3 and S5 and S8 are "ON". The four switching combinations can be seen in Fig. 2.3 and will be defined based on when the circulating current is positive for "Sequence 1". After that whenever the circulating current changes polarity the sequence increases, and thereby the sequence follows: 1-2-3-4-1. As the measurements in Fig. 2.3 are scoped in SS then these measurements will repeat themselves until the simulation is terminated.

Although the circulating current illustrated in Fig. 2.3 appears to be uni-directional, but it has a negative component that can not be seen in the figure due to its scaling. The negative circulating current has a peak of about $2.5[mA]$, which is low compared to the positive peak of $0.88[A]$. According to the four switching combinations illustrated in Fig. 2.3, the corresponding circuit diagram for each sequence are illustrated in Fig. 2.4, 2.5, 2.6 and 2.7 respectively.

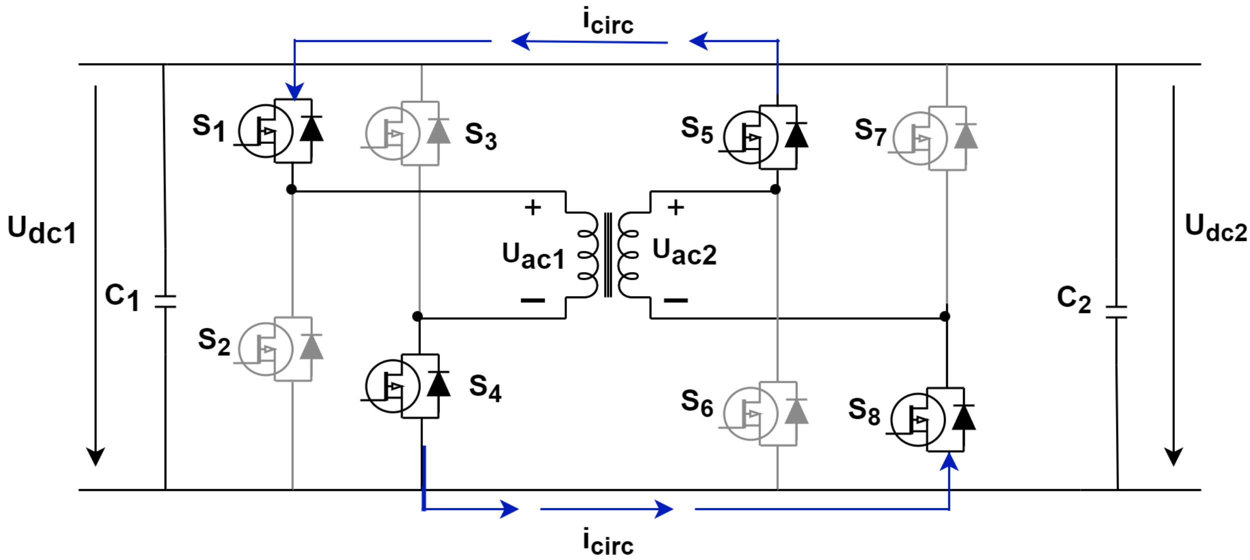

Figure 2.4: Circulating current path during sequence 1

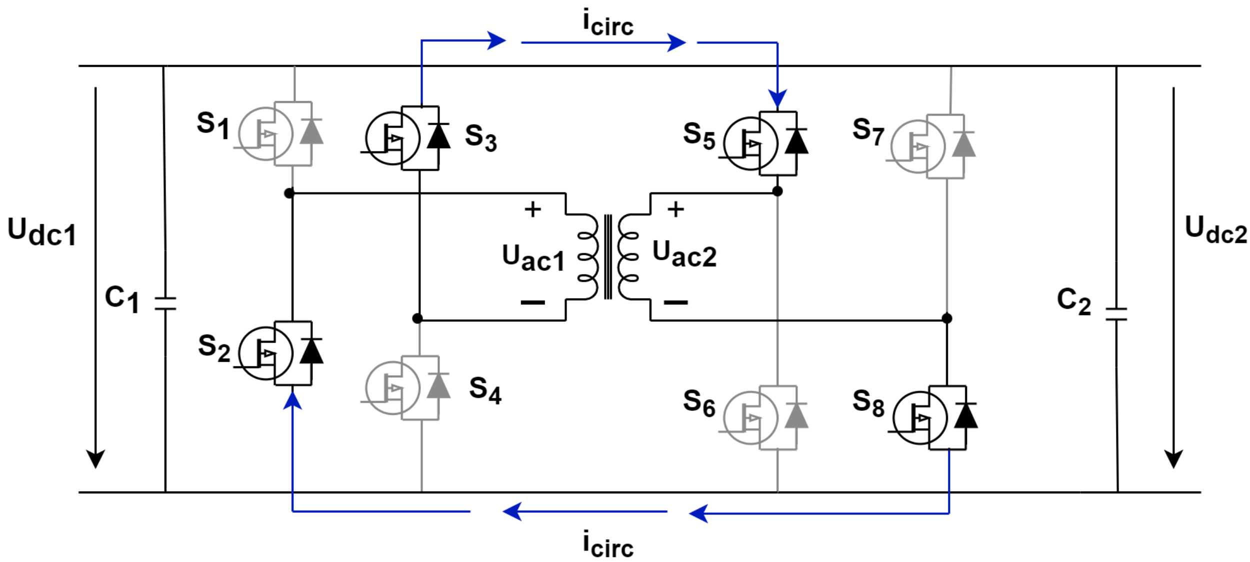

Figure 2.5: Circulating current path during sequence 2

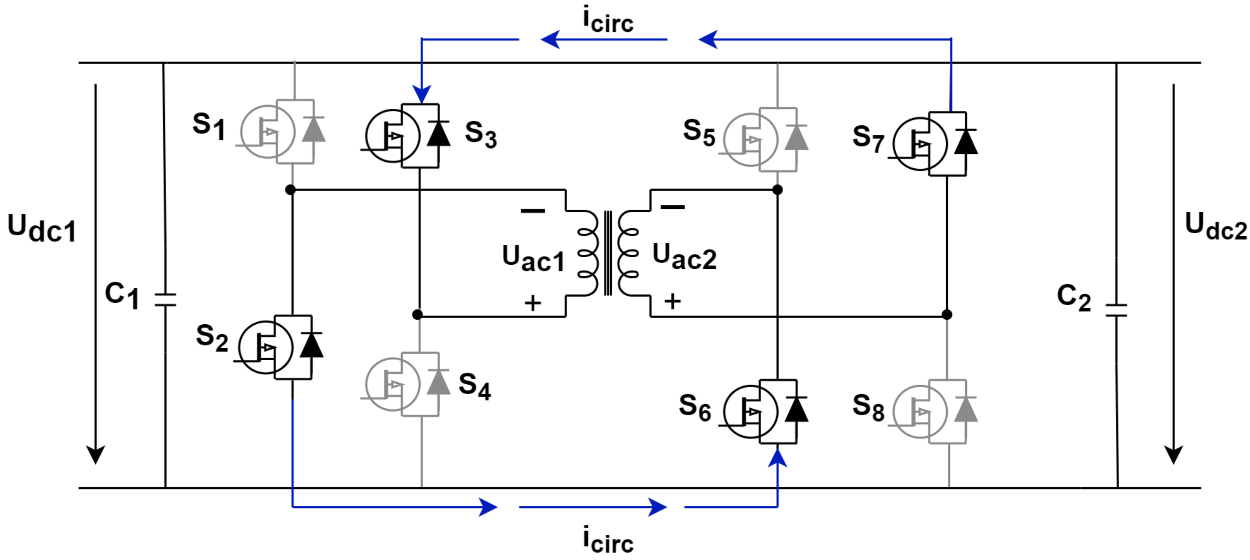

Figure 2.6: Circulating current path during sequence 3

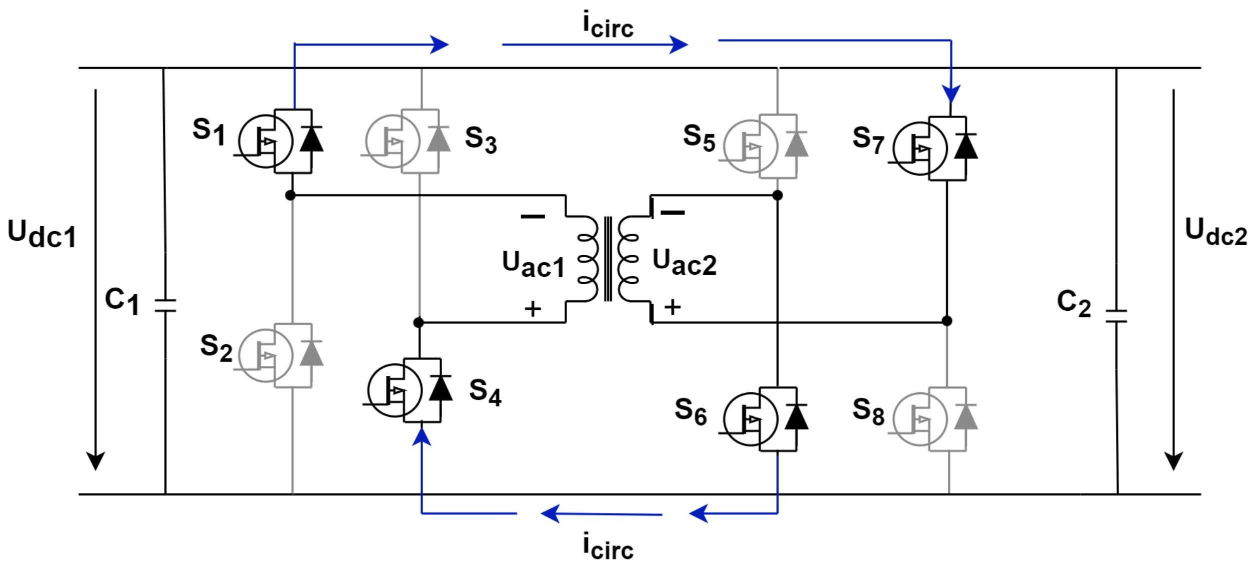

Figure 2.7: Circulating current path during sequence 4

Thereby, depending on the applied switching combination, the polarity of the AC transformer voltage and the direction of the circulating current changes, as illustrated in the above four figures.

By further testing the system, it is discovered that the different parameters of the system affected both the waveform and magnitude of the circulating current. Therefore by utilizing the circulating current path, it becomes possible to control the power flow of the system. Furthermore, depending on the magnitude of the phase-shift applied between the primary and secondary converter's gating signals, the circulating current (i_{circ}) changes. This includes the current's peak magnitude and direction.

With both the different types of operation principles and the circulating current path introduced and discussed, then modelling and simulations of the system can be conducted. This will be performed in the following Chapter.

Chapter 3

Simulation - Open-Loop Control

With the introduction and theoretical analysis of the DAB circuit from the previous chapter, this chapter focuses on a theoretical testing of a high-frequency transformer as the Device Under Testing (DUT), which is the high-frequency transformer, will be the focus of this chapter. First, a starting point for the applied parameters will be given, and afterwards, these will be used in order to test the system. The system will be tested in regards to the applied switching topology by changing the applied switching frequency, phase-shift and duty cycle. Based on the results, it is looked into whether improvements to the performance of the testing system can be achieved.

The complete simulation circuit based on the DAB topology is presented in Fig. 3.1. There are certain components added to the DAB circuit for the realistic practical operations. U_{dc1} and U_{dc2} are the input and output DC voltages and their values are set as per the requirements described in Table 1.1.

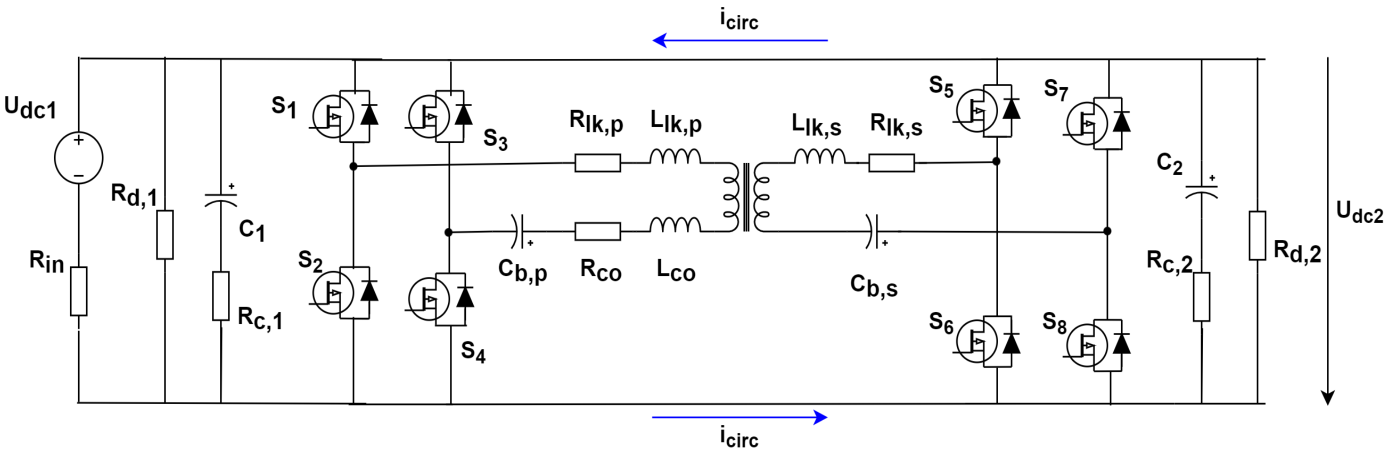

Figure 3.1: DAB simulation circuit

At the input side, R_{in} is the input source resistor used to increase the impedance at the power supply side so that maximum current can flow through the capacitor C_1. C_1 is the capacitor used to smoothen the voltage ripples. $R_{d,1}$ is a resistor connected parallel to C_1. It is used for the protection of the circuit. It provides C_1 a path to discharge the extra energy when a short circuit occurs across the primary side or when the input source is turned off. $R_{C,1}$ is the series-connected resistor to the C_1. It is also used for the safety of the circuit. If any short circuit occurs in the circuit, this resistor generates a time constant to give the short time protection to the circuit.

On the primary side, $L_{lk,p}$ and $R_{lk,p}$ are the internal leakage inductance and resistance of the transformer, respectively. R_{co} and L_{co} are the resistance and the inductance connected to the primary side and used to limit the AC current. $C_{b,p}$ is the capacitor to block the DC voltage and thereby provide voltage protection for the primary side of the transformer. On the secondary side of the transformer, an inductor $L_{lk,s}$, resistor, $R_{lk,s}$ and capacitor $C_{b,s}$ are connected. The function of these components are identical to the $L_{lk,p}$, $R_{lk,p}$, $C_{b,p}$ respectively. Also, the capacitor C_2 is present to reduce the voltage ripples, and $R_{c,2}$ and $R_{d,2}$ are for protecting the circuit at the output side with the same function as their input side representation.

The value of the system parameters will be given in the following before the testing will be conducted.

3.1 System parameters

The parameter applied for the complete system circuit, shown in Fig. 3.1, are given in Table 3.1.

Table 3.1: System parameters

System	Description	Notation	Value	Unit
Transformer	Leakage inductance	$L_{lk,x}$	10	$[\mu H]$
	Leakage resistance	$R_{lk,x}$	0.1	$[\Omega]$
4-Switch Converters	Switching frequency	f_{sw}	250	$[kHz]$
	Duty cycle	δ	50%	$[-]$
	Phase-shift	D	80	$[^o]$
Protection	Blocking capacitor	$C_{b,x}$	2	$[\mu F]$
	Smoothing capacitor	C_y	100	$[\mu F]$
	Input source phase resistor	R_{in}	5	$[\Omega]$
	Capacitor's series resistor	$R_{c,y}$	1.5	$[m\Omega]$
	Dissipation resistor	$R_{d,y}$	800	$[k\Omega]$
Control	Control inductor	L_{co}	2	$[mH]$
	Control resistor	R_{co}	0.01	$[\Omega]$

In Table 3.1, the subscript "x" refers to a primary and secondary transformer parameter with the same value, and "y" refers to the input and output parameters. In addition, for the simulation model for this project, the initial voltage across the two smoothing capacitors, C_y, is the same and equal to the value of the input DC voltage source.

By applying the parameters given in this section, the testing of the system will be performed. In the following sections, the system will be tested by focusing on one parameter and varying it in order to illustrate its influence on the system performance. Therefore in this chapter, an "open-loop control" will be applied for the system, which will contribute to realizing a "closed-loop control". The tested parameters are the switching frequency, phase-shift and duty cycle. For the following test of the system, the SPS control will be implemented, although the duty cycle will be kept at the initial value of 50% with the exception of one of the tests where it will be changed. In addition, only the SS results within one switching period will be illustrated, as the initial transient will not occur in the experimental testing where the input voltage increases gradually from zero to the required voltage level. The focus of this report is the operating conditions of the transformer and the circulating current path then, the smoothing capacitor current will not be illustrated. The same applies to the output voltage unless a significant change occurs.

3.2 Testing analysis at different Switching frequency values

To test the influence of the switching frequency, f_{sw}, the system will be tested at five different frequencies. The chosen switching frequencies are 10 [kHz], 50 [kHz], 100 [kHz], 175 [kHz] and 250 [kHz]. Thereby, the system performance will be tested, and the robustness of the switching between the converter switches has been examined for the changing frequencies. The results shown are not for the one switching period as the values of the frequency is changing.

While simulating the system for this test, voltage signals are kept the same and will therefore not be illustrated. These signals are the input and the output voltage (primary and secondary voltage). Also, there is a small increase in the leakage inductor voltage. However, it is only a few volts and therefore negligible. In addition, the output voltage ripple showed an inverse proportional increase to the switching frequency. However, they are in the range of a few volts. which is negligible compared to the magnitude of the voltage. Therefore, only the primary leakage inductor current and the circulating current are illustrated in this test. First the primary leakage current will be illustrated, which is given in Fig. 3.2. Where in Fig. 3.2a, the primary leakage inductor current for all tested switching frequencies is illustrated, and in Fig. 3.2b, the three results with the lowest currents are illustrated.

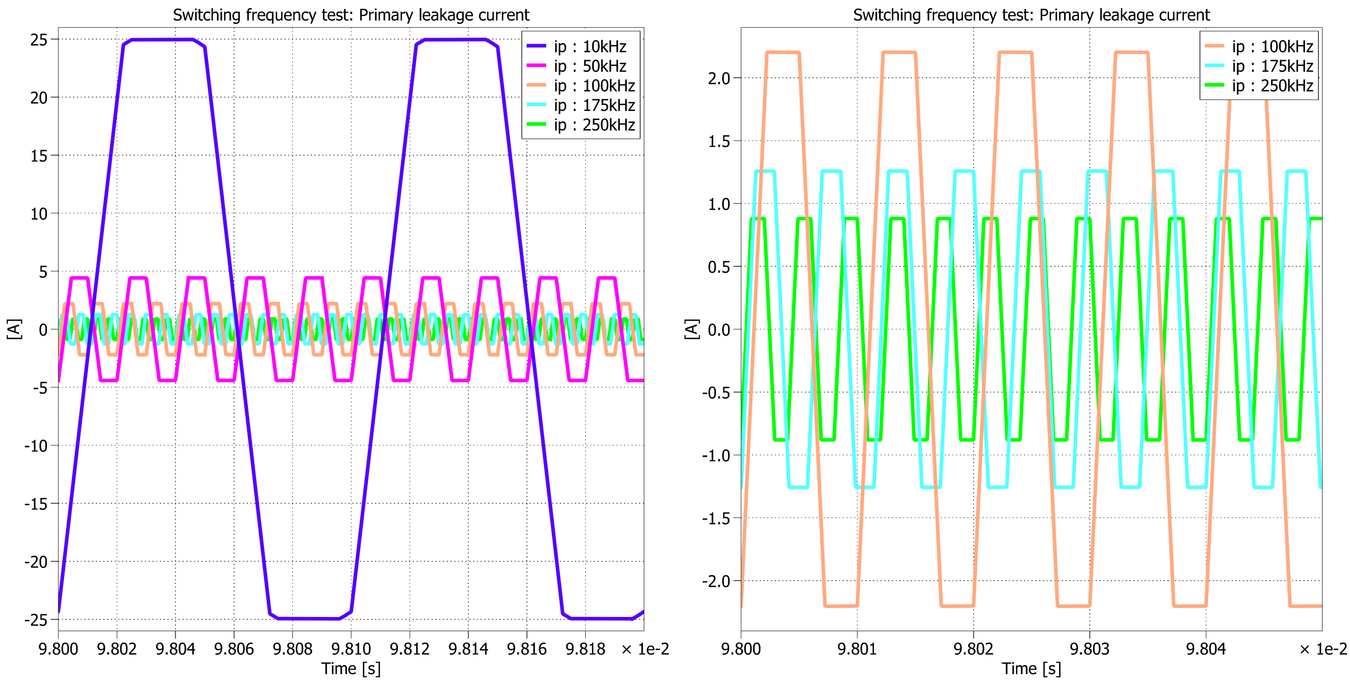

(a) All results **(b)** Zoomed in results

Figure 3.2: Switching frequency test: Primary leakage inductor current results

From Fig. 3.2, it can be seen that the amplitude of the primary leakage inductor current is inversely proportional to the switching frequency. Therefore, as the frequency increases, the amplitude of the AC primary leakage inductor current will decrease. Also, the change in the switching frequency have no influence in regards to the waveform of the leakage current except for its amplitude. In addition, it is observed that the amplitude of the primary voltage is inversely proportional to the value of frequency.

The resulting circulating currents for the switching frequency test are illustrated in Fig. 3.3. In Fig. 3.3a, the circulating current for all tested switching frequencies is illustrated, and in Fig. 3.3b, the three results with the lowest currents are illustrated.

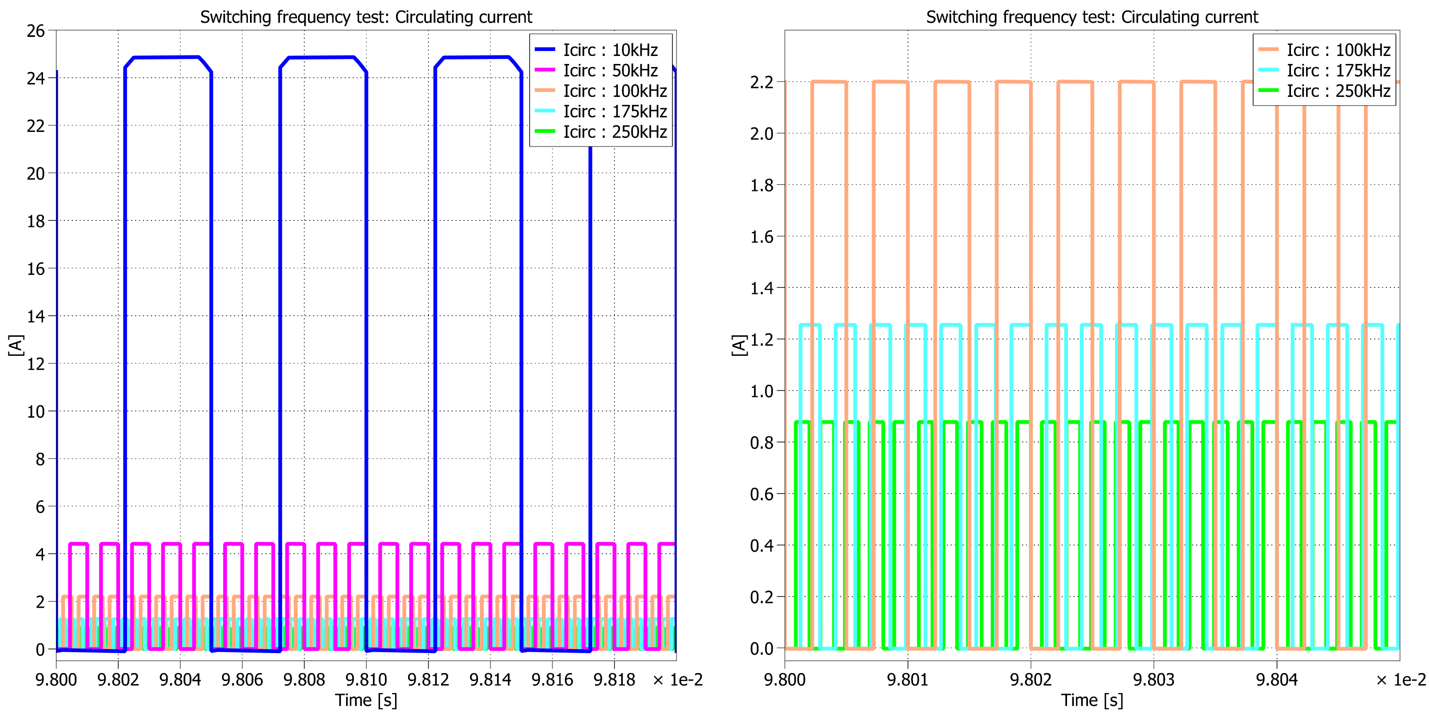

(a) All results **(b)** Zoomed in results

Figure 3.3: Switching frequency test: Primary leakage inductor current results

As shown in Fig. 3.3, the amplitude of the circulating currents follows the same pattern as the primary leakage current in regards to the change in frequency. The results in both Fig. 3.2 and 3.3 are measured in the same time frame. It can be seen that when the circulating current reaches its positive peak, the primary leakage inductor current is either at its positive or negative peak. Therefore the positive circulating current contributes to the current of the primary side within its positive period. In SS the input current's peak is at a few hundred [mA] at the lowest frequency. Therefore, the primary leakage inductor current is mainly supplied by the circulating current.

3.3 Testing analysis at different phase-shift values

To further test the system, the phase-shift, D, is changed for the gating signals of the two four-switch converters. The phase-shift will be tested at three different values and in addition at two different switching frequencies. The system will be tested with a phase-shift of 40°, 80° and 120° with a switching frequency of 250 [kHz] and 10 [kHz] respectively. The phase-shift test results will be split into two subsections based on the tested switching frequency. First, the 250 [kHz] test will be shown.

3.3.1 250 [kHz]

While simulating the system at different phase-shift it is discovered that negligible change occurred in all signals except the primary leakage inductor current and the circulating current. Therefore, only primary leakage inductor current and circulating current will be illustrated. In Fig. 3.4 the phase-shift test results are illustrated. Whereas, in Fig. 3.4a the primary leakage inductor currents are illustrated, and in Fig. 3.4b the circulating currents are illustrated.

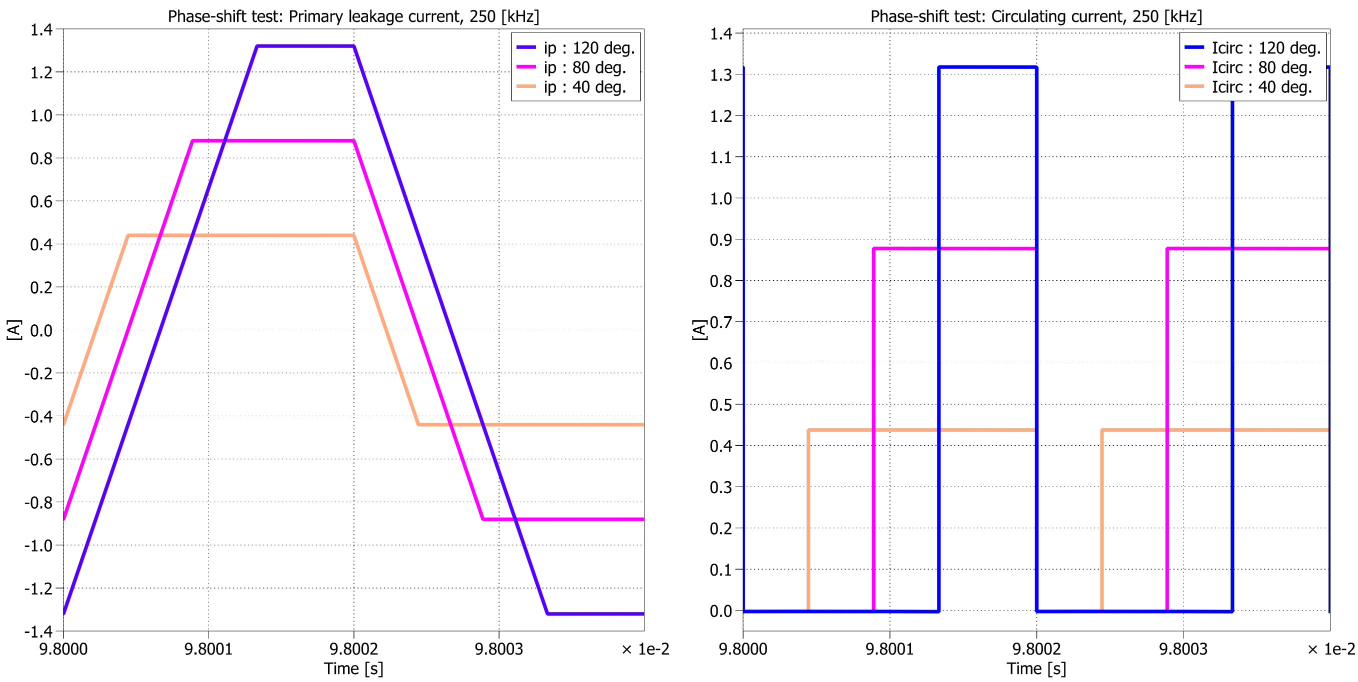

(a) Primary leakage inductor current

(b) Circulating current

Figure 3.4: Phase-shift test: 250 [kHz] results

From Fig. 3.4a it can be seen that the higher phase-shift between the gating signals of primary and secondary 4-switch converter is, the higher the amplitude of the primary leakage inductor current becomes. The same tendency can be seen on the amplitude of the positive peak of the circulating current, as shown in Fig. 3.4b, while the negative peak of the circulating current has negligible change. Therefore, the amplitude of the currents is proportional to the phase-shift. Since, at 250 [KHz] switching frequency, the current magnitude is at its lowest value. It is relevant to test with a different switching frequency where the amplitude change becomes significant.

3.3.2 10 [kHz]

The phase-shift test is also performed at 10 [kHz] to study if the tendency occurs at a different switching frequency. The primary leakage current and the circulating current are measured with the new switching frequency. The results of the test are illustrated in Fig. 3.5. In Fig. 3.5a the primary leakage inductor currents are illustrated, and in Fig. 3.5b the circulating currents are presented.

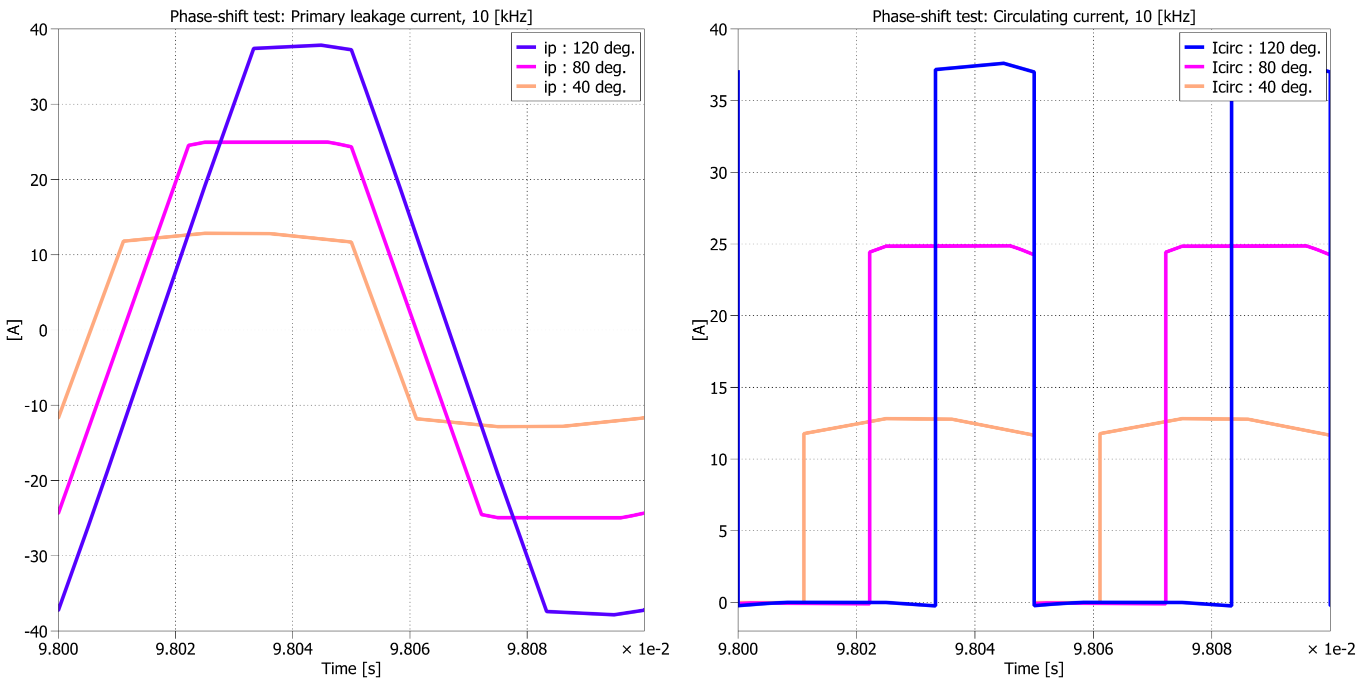

(a) Primary leakage inductor current

(b) Circulating current

Figure 3.5: Phase-shift test: 10 [kHz] results

From Fig. 3.5a and 3.5b the same tendency as with the $250[kHz]$ test can be seen as the magnitude of the current signals increases as the phase-shift becomes larger. In addition, as seen in Fig. 3.5b the positive part of the circulating current has a hill shaped response at the low phase-shift value compared to the flat shape at the higher values. As it can be seen at the lower switching frequency, the change in the phase-shift results in a significant change in the magnitude of the currents.

3.4 Testing analysis at different duty cycle values

Although the SPS control, introduced in Section 2.1.1, is with a fixed duty cycle of 50%, this system will be tested at different duty cycle value in order to further analyse the controllability of the transformer conditions. Like the test of the variable phase-shift, every duty cycle values will also be performed with the same switching frequencies. Therefore, the system will be tested at five different duty cycle and a switching frequency of 250 [kHz] and 10 [kHz], respectively. The tested duty cycles are 10%, 30%, 50%, 70% and 90%. Like the phase-shift test, the duty cycle test results are also split into two subsections based on the tested switching frequency. First, the 250 [kHz] test will be shown.

3.4.1 250 [kHz]

Same as the phase-shift, the change in the duty cycle only showed significant changes in the primary leakage inductor current and the circulating current. In Fig. 3.6 the duty cycle test results at a switching frequency of 250 [kHz] are illustrated. In Fig. 3.6a the primary leakage inductor currents are illustrated, and in Fig. 3.6b the circulating currents results are presented.

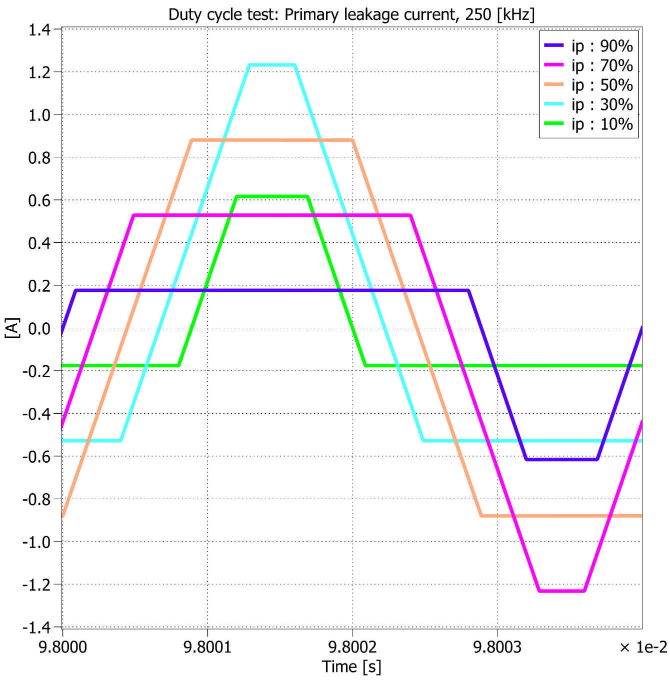

(a) Primary leakage inductor current

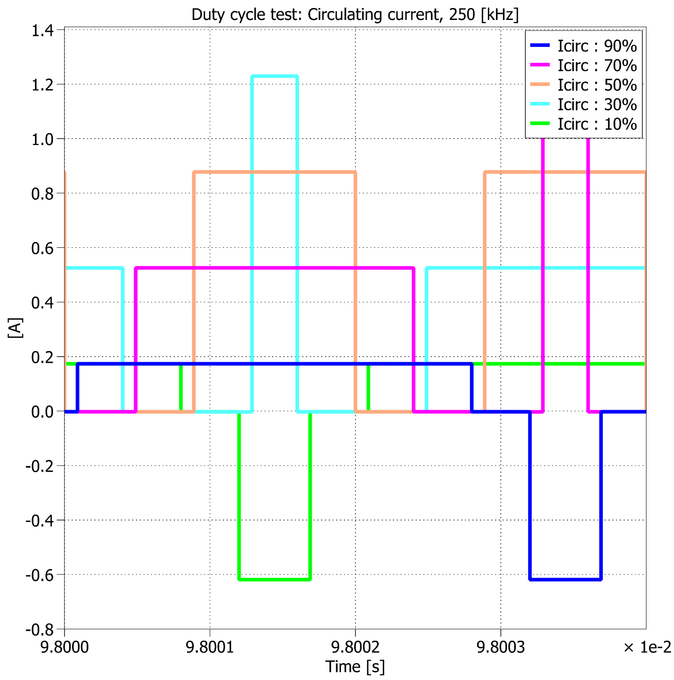

(b) Circulating current

Figure 3.6: Duty cycle test: 250 [kHz] results

As illustrated in Fig. 3.6a, the values different from the standard 50% duty cycle results in a unsymmetrical waveform for the primary leakage inductor current. Therefore, the period where the smoothing capacitors store and discharge energy no longer remains the same. At the positive peak, increasing the duty cycle from 50%, results in a lower peak in the primary leakage inductor current. Therefore, the negative peak should be more concentrated and have a higher peak and higher the duty cycle. However, this pattern does not appear as the measurement at the 90% have a small negative peak from the 50% while the 70% have a higher negative peak. This might be due to the discharging period being too low to fully make use of the charged energy of the smoothing capacitor. While lowering the duty cycle from the standard 50%, the opposite pattern occurred. Therefore, the 10% and 30% measurements are equivalent to a mirror image of the measurements at 90% and 70% respectively.

In the case of the circulating current, it shows the same pattern as illustrated in the previous tests. When the primary leakage inductor current has either a positive or negative peak, the circulating current has a positive value of approximately the same amplitude. However, this pattern does not occur at the lowest and highest tested duty cycle values, as illustrated in Fig. 3.6b. Therefore, additional energy will be returned to the secondary side of the transformer compared to previously, where most of the circulating current is used to supply the primary side current. Thereby, it is observed that by controlling the duty cycle, the energy flow of the system can be controlled.

In order to illustrate the significance of changing the duty cycle, the duty cycle test is conducted with a smaller switching frequency, which, based on previous tests, resulted in a higher current amplitude. Therefore, the duty cycle test will be performed with a switching frequency of 10 [kHz] in the following.

3.4.2 10 [kHz]

With the new switching frequency, the primary leakage inductor current and the circulating current are measured again. In Fig. 3.6 the duty cycle test results at a switching frequency of $10[kHz]$ are illustrated. Where in Fig. 3.7a the primary leakage inductor currents are illustrated, and in Fig. 3.7b the circulating currents results are given.

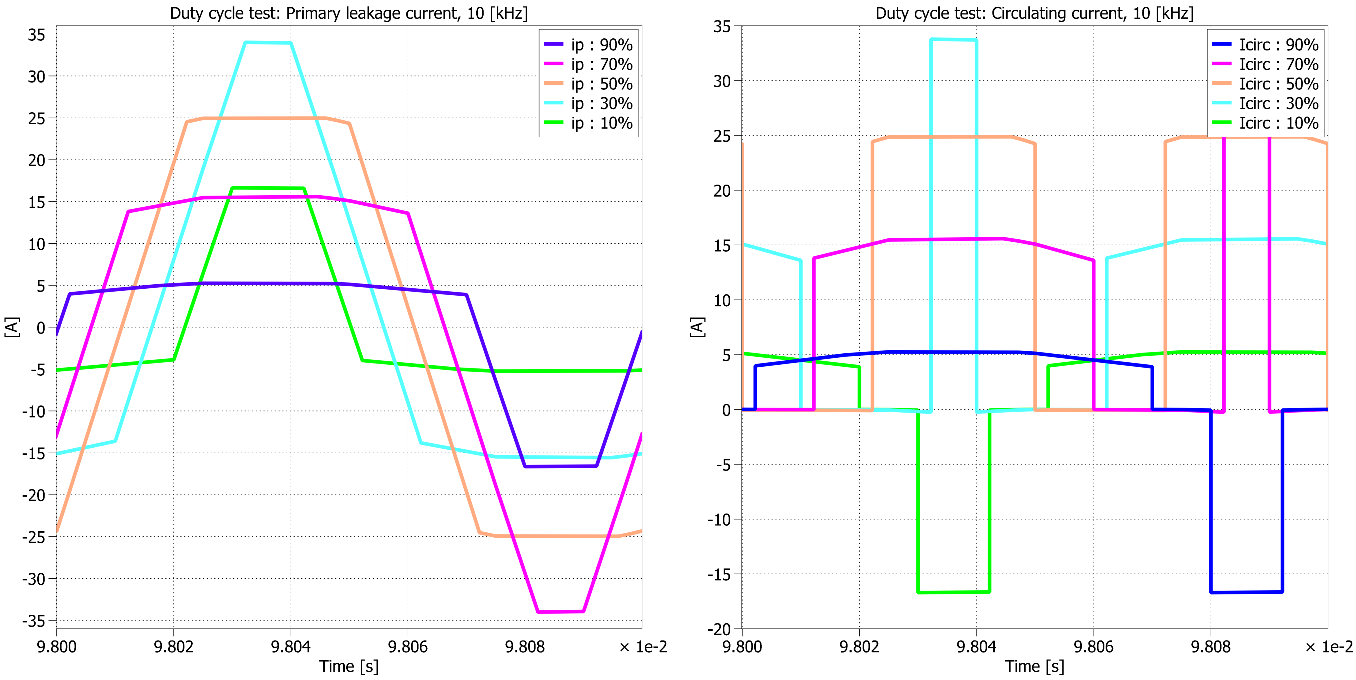

(a) Primary leakage inductor current

(b) Circulating current

Figure 3.7: Duty cycle test: 10 [kHz] results

Like the previous tests, lowering the switching frequency results in a significant increase in the amplitude of the current signals as illustrated in Fig. 3.7a and 3.7b. In addition, the results in Fig. 3.6 and 3.7 has the same pattern while changing the duty cycle. The comparison of two duty cycle tests has been performed, changing the duty cycle by 20% results in an amplitude change of $10[A]$ for the $10[kHz]$ duty cycle test. In contrast, for $250[kHz]$ duty cycle test where the current amplitude is only a few hundred $[mA]$.

By utilising the results of the tests performed in this Chapter, a "closed-loop control" for the system can be realised. This will be derived in the following Chapter.

Chapter 4

Simulation – Closed-Loop Control

In order to improve the performance of the system described in chapter 3, a closed-loop control system is required. It is also needed in order to validate the performance on the hardware setup. This Chapter focuses on the structure and design of a closed-loop control system. The simulated results of the designed system are also presented and explained. In Chapter 3 the controllable parameters are the phase-shift and the duty cycle. However, the main focus of this project is to control the conditions of the DUT and the phase-shift has the most influence on the amplitude of the transformer current. Therefore the duty cycle will be fixed while a closed-loop control will be derived to control the current by changing the phase-shift. The closed-loop control system is to ensure that the transition of the current from one value to another value will be smooth and accurate. The closed-loop system also minimizes the overshoot and aid the system to perform at sufficient speed.

4.1 Structure

Basic block diagram of the closed-loop structure is shown in Fig. 4.1. The reference current I_{ref} and the Root-Mean-Square (RMS) primary current $I_{p,rms}$ is compared and the current error I_{error} is generated. This error is then removed with the help of Propotional-Integral (PI) controller that generates the required phase-shift D. The required phase-shift is then applied to the plant, which is a representation of the DAB system, for accurate operation.

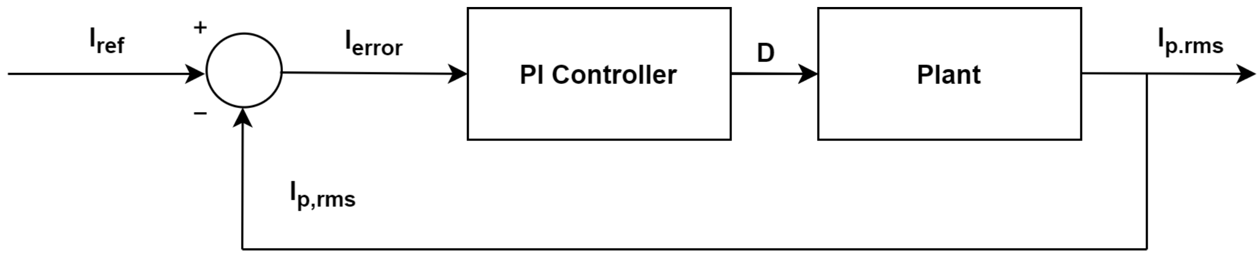

Figure 4.1: Overview of phase-shift closed-loop control

The phase-shift controller is to generate the required phase-shift in order to control the current precisely. Fig 4.2 shows the modelled structure of the closed-loop control. I_{error} is generated by comparing $I_{p,rms}$ and I_{ref}. I_{error} is then fed to the Zero Order Hold (ZOH) block. The ZOH block is used for the continuous to discrete signal conversion as the PI controller is a discrete-time controller. After the sufficient tuning of the PI parameters, the required phase-shift D is generated. The phase-shift and the constant 50% duty cycle δ are applied to the gate signal generator to produce the required gating signals for the transformer switches.

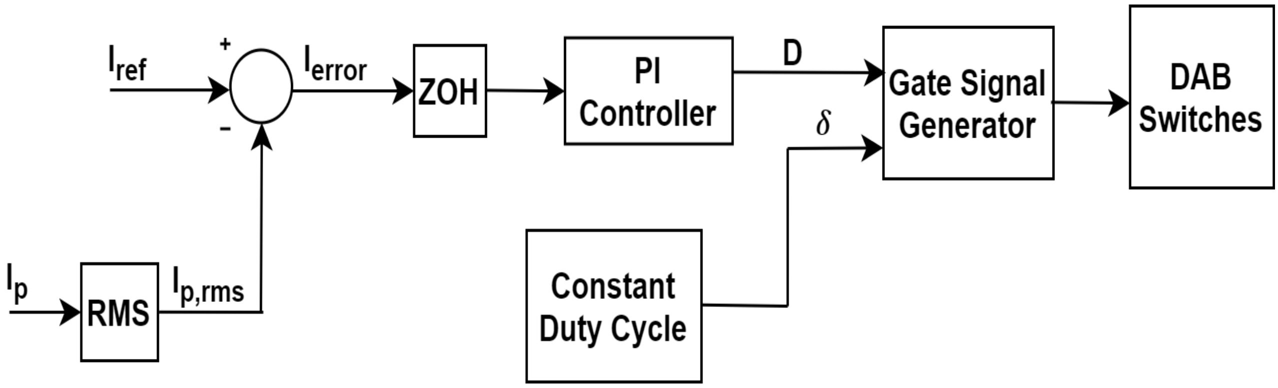

Figure 4.2: Modelled phase-shift controller

Fig. 4.3 illustrates the structure of the gate signal generator. ON carrier block detects and gives the information to the PWM signal generator to turn the DAB switches ON. The function of the ramp shifter is to shift the ON carrier signal for certain degrees depending on the duty cycle δ in order to generate the OFF carrier. The OFF carrier, on the other hand, instructs the PWM signal generator to turn OFF the required switches.

D is the phase-shift fed to the saturation block. D is measured in degrees. The saturation block is used as a safety feature to avoid the PWM being locked at either 1 or 0 due to the internal structure of the PWM signal generator block. K is the factor that is multiplied in order to make the phase-shift as scalar value to accommodate the requirements of the PWM signal generator. The PWM signal generator then generates the required gating signal for the switches of the primary and the secondary side converters.

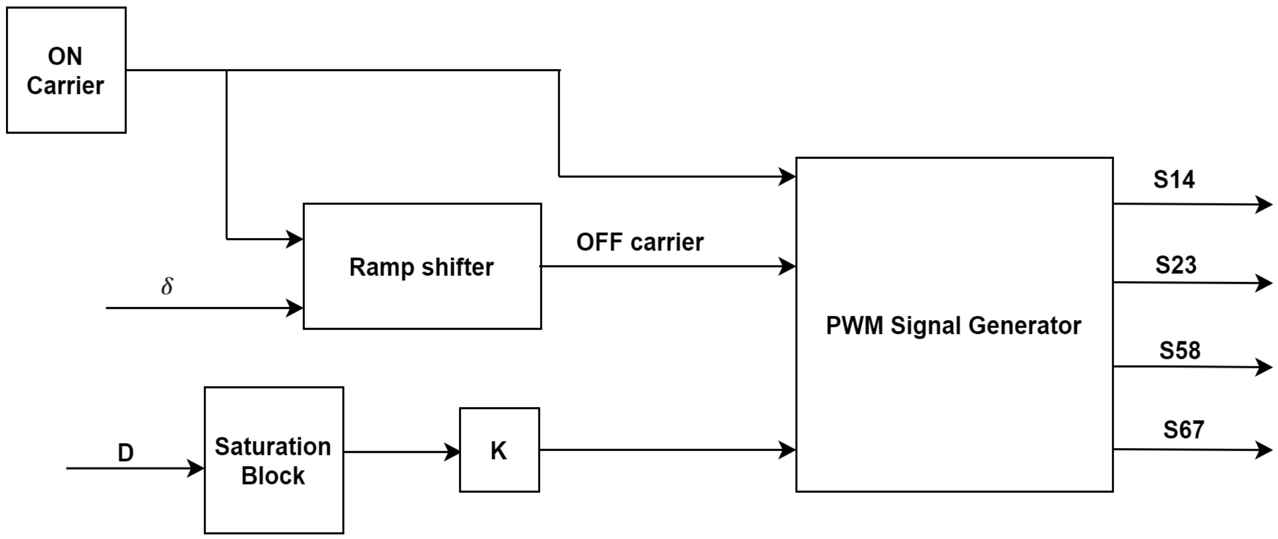

Figure 4.3: Gate signal generator

The phase-shift controller is tuned for the system operation. First, the current reference is fixed and then the controller tuning is performed. The details about the phase-shift control tuning are discussed in the Section below.

4.2 Phase-shift control

Generally, there are two methods to tune the PI parameters of the controller for the closed-loop system in Fig. 4.1. One way is to build the system transfer function and tune the PI parameters by the transfer function responses. Another way is to perform the tuning based on a trial-and-error approach from the simulation responses. For simplicity, the PI parameter tuning of the phase-shift controller for this project is performed by a trial-and-error approach based on simulation responses. For the model, the sample time for both the ZOH and the discrete PI controller will be the same, and it is equal to $2/f_{sw}$.

For the manual tuning of the phase-shift control, the current reference will be set to be equal to the maximum transformer AC peak current of 20 [A] in accordance to Table 1.1. Based on the results from Chapter 3, the amplitude of the transformer AC current increases in the lower frequency range. Therefore the controller tuning will be performed using 10 [kHz] as the switching frequency. As the feedback of the phase-shift control is the RMS of the primary current, then the peak reference will need to be referred to RMS. As an assumption for the manual controller tuning, the primary current is considered a symmetrical square-wave signal. Therefore the peak current reference is considered to be equivalent to the RMS value. From Chapter 3 the primary current is illustrated under different conditions, and as shown, the waveform is not a symmetrical square wave. Therefore, it should be noted that the RMS value in the model will be lower than the actual RMS value, and thereby the measured peak of the primary current will be higher than the peak based on the assumption.

Before the tuning can be performed, a few changes to the simulation model are necessary. As the phase-shift have limitations in regards to its magnitude, the model is modified such that the controller output is in the range of ± 180 [^{o}]. The gating signals modelling is initially required to be in the range of ± 0.5, therefore the value of the factor K equals $1/360$ [^{o}] in order to achieve this. Thereby the range of the controller output is expanded. In addition, an appropriate value for the fundamental frequency of the RMS block is chosen. Preliminary testing shows that increasing the fundamental frequency results in a faster response. However, it also results in unwanted oscillations of the output signal, which increased with the frequency. From this, a value of 200 [Hz] for the fundamental frequency of the RMS block results in an acceptable response.

4.2.1 K_p tuning

For all tests in the following, the current reference for the phase-shift control will be stepped from 0 to the reference value when $t = 0.03$ [s]. To start, the proportional gain of the PI controller is varied, while the integral gain is zero. Therefore it is chosen to simulate the system with the phase-shift control at 6 different K_p values: 12, 9, 8, 5, 2 and 0.2 [-], respectively. The current responses using these proportional gains are illustrated in Fig. 4.4.

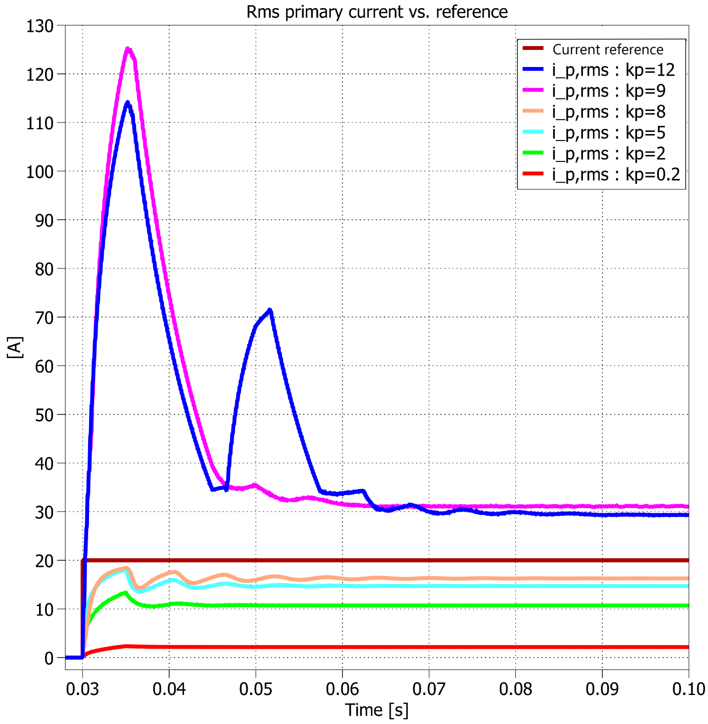

Figure 4.4: RMS feedback current vs. reference

From Fig. 4.4, all current responses will reach a SS value despite the transient oscillations. However, the high overshoot for the proportional gains above eight peaks at a point several times the reference current. This will practically be an issue as the transformer will have a current limit. In addition, these overshoots violate the set maximum current peak for this project. The effect of these overshoots will be directly affecting the performance of the controller, which can be seen by the controller response. The controller responses for the different proportional gains are illustrated in Fig. 4.5.

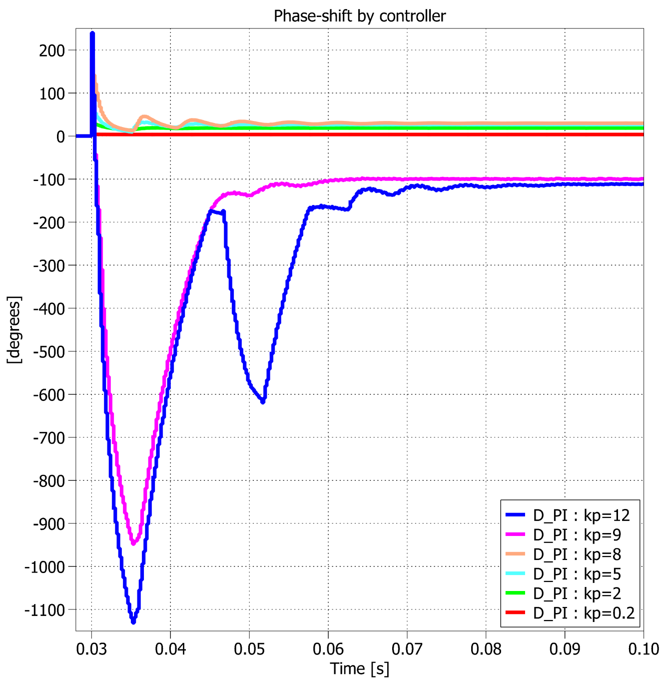

(a) Controller output

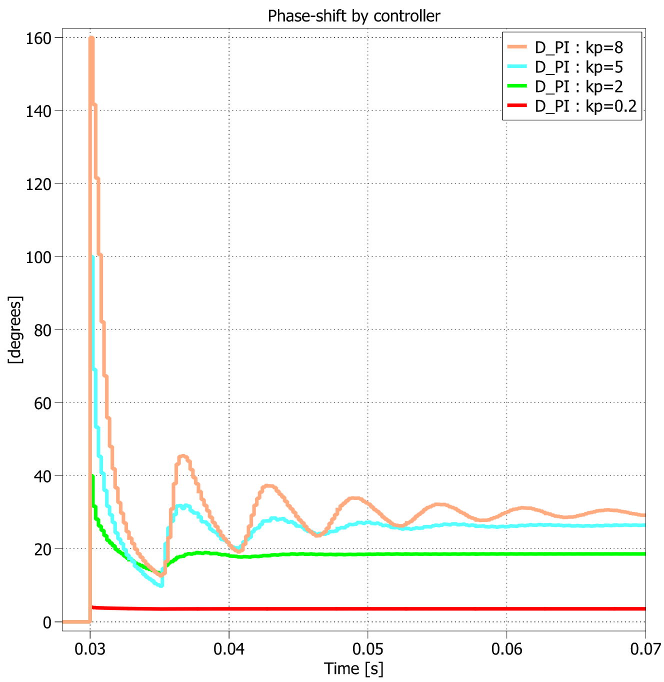

(b) Controller output (Zoom)

Figure 4.5: Controller response by K_p change

From Fig. 4.5, the initial phase-shift after the step is equivalent to the product of the reference and the applied proportional gain. Since the modelled gating signal generator is limited to a phase-shift in the range of $[-180; 180]$, then there is a threshold value for the proportional gain. This effect can be seen in Fig. 4.5a for the results using $K_p = 9$ and $K_p = 12$ as it results in a negative phase-shift, which is undesirable. From Fig. 4.5b the results for the results below the threshold of K_p are illustrated. It can be seen that the lower the K_p, the lower the initial phase-shift and less oscillations. The high initial phase and transient oscillations are undesired as they have an equivalent effect on the primary current and, therefore will need to be removed. However, by only using a proportional gain for the control, there is no way to remove the undesired behaviour. Therefore the integral gain will be increased.

4.2.2 K_p and K_i tuning

In order to choose a suitable integral gain then the control is tested with four different integral gains. The integral gain is fixed at either 1000, 500, 300 or 100 for the controller tuning. For an initial value of the proportional gain, it is chosen as 5. The responses of the feedback RMS current for the different integral gains are illustrated in Fig. 4.6.

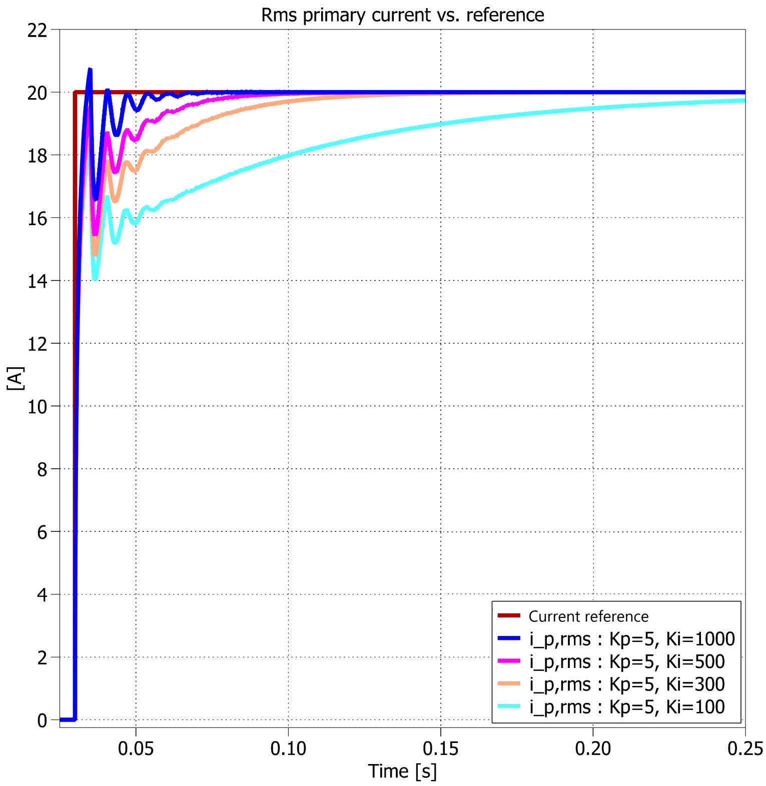

Figure 4.6: RMS feedback current vs. reference

Since the control now includes an integral, the feedback follows the reference and reaches SS, as illustrated in Fig. 4.6. With the proportional gain of 5, there are minimal changes to the transient oscillations despite an increase in the integral gain. In addition, no current overshoot occur with this proportional gain for all tested integral gains. Although minimal changes occur to the transient oscillations, an increased integral gain resulted in a faster current response. By the closed-loop phase-shift control, a smaller phase-shift can be applied to obtain the similar amplitude of the primary contrary to the open-loop testing performed in Section 3.3.

Following the effect of the integral gain, the controller response is given. The resulting controller responses for the test are illustrated in Fig. 4.7.

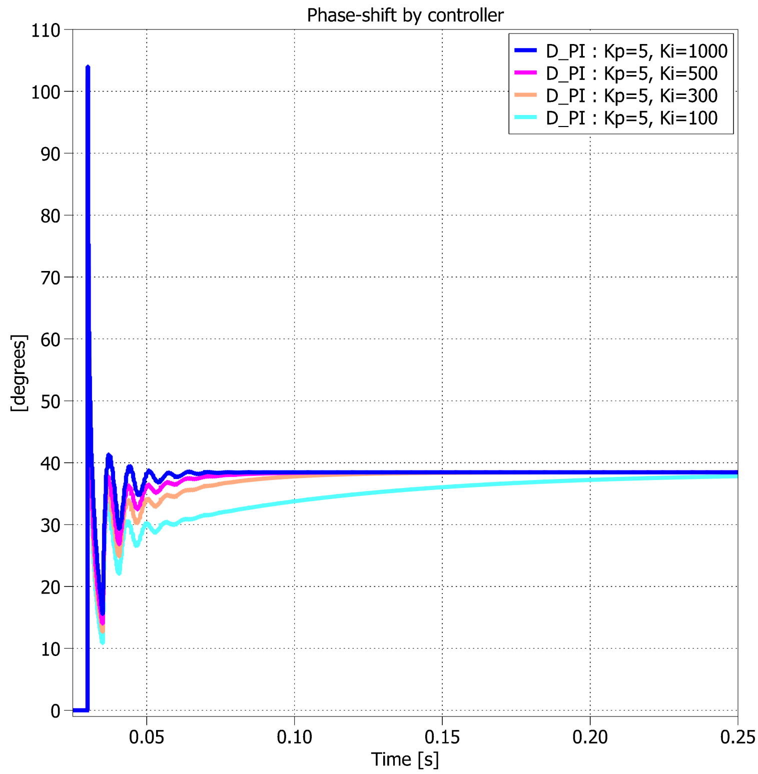

Figure 4.7: Controller response by $K_p = 5$ with different K_i

From Fig. 4.7, contrary to the current response, the controller responses have an issue in regards to the initial phase-shift after the step. The transient follows the same waveform as the current response. The initial phase-shift overshoot might be an issue that need to be overcome. As the initial phase-shift is directly equal to the product of the current reference and the proportional gain, the proportional gain for the phase-shift controller is reduced, and the integral gain test is performed again. Therefore the proportional gain is changed to 0.2 [-]. The current responses with the new proportional gain are illustrated in Fig. 4.8.

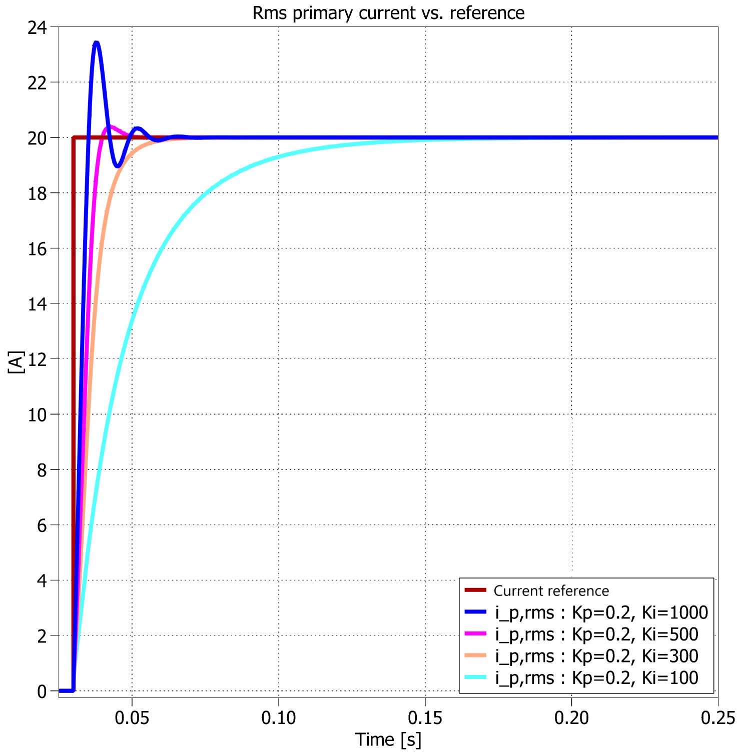

Figure 4.8: RMS feedback current vs. reference

With the new proportional gain, the transient of the current response is more smooth. Although there is an overshoot in the response for the two highest integral gains, they reach SS faster than the other current responses in Fig. 4.8. Now the control response is examined before the tuning of the phase-shift controller at 10 [kHz] is concluded. The control responses are illustrated in Fig. 4.9.

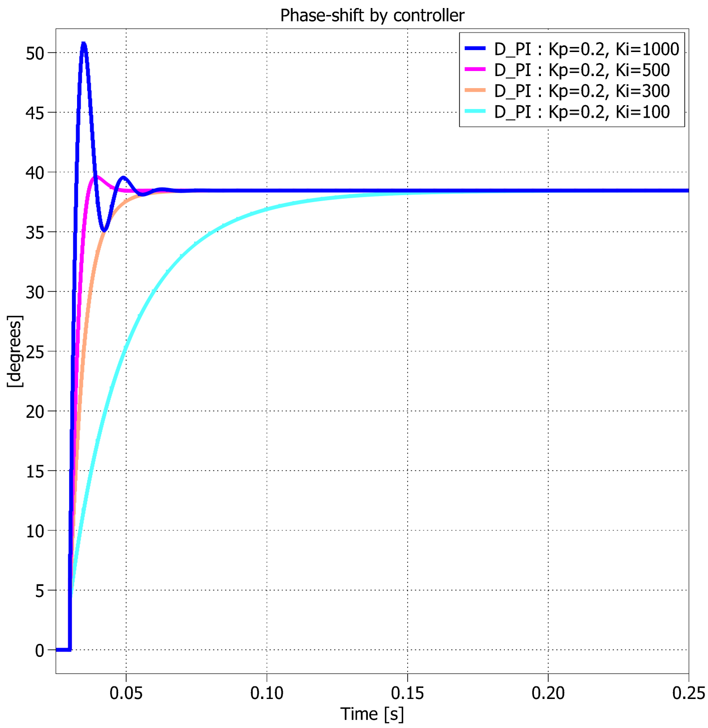

Figure 4.9: Controller response by $K_p = 0.2$ with different K_i

Contrary to Fig. 4.7, the large initial phase-shift is reduced and the transient have become more smooth, as shown in Fig. 4.9. As it is unwanted to have overshoot and oscillations in the transient response, then a proportional gain of 1000 and 500 can be excluded for the potential proportional gain. Although requirements to the SS response time have not been given, it is chosen to have the integral gain with the faster response. Therefore an integral of 300 is chosen for the phase-shift at 10 [kHz]. Thereby, the manual tuning of the phase-shift controller is concluded. The continuous transfer function of the tuned controller is presented in Eq. 4.1.

$$C_D(s) = K_p + K_i \cdot \frac{1}{s} = 0.2 + 300 \cdot \frac{1}{s} \tag{4.1}$$

By utilising the tuned controller, the system performance is improved. As the system modelling is in the discrete domain, then within the PLECS modelling [13] the PI controller is discretised. With the discretised controller, the system performance is tested to its response to a change in the switching frequency and current reference.

4.3 Testing with stepped current reference

For the testing performed in this section, the current reference is stepped to different values. The initial step will remain to occur when $t = 0.03$ [s] and the current reference is changed again when $t = 0.2$, and thereafter, the current reference is changed every 0.2 [s]. First, the testing is performed with a switching frequency of 10 [kHz]. Thereafter the tuned controller is tested with a switching frequency of 250 [kHz] in order to its performance at a frequency different from the tuned.

4.3.1 10 kHz

The current reference is changed in the following order: $20 \rightarrow 10 \rightarrow 5 \rightarrow 0 \rightarrow 20$ [A], where the first value is after the initial step. While testing the controller performance with the several steps in the current reference, the closed-loop control has an issue when the reference is returned to be 0. In order to solve this issue, the lower limit of the saturation block is changed from -180 to be 0. The current responses with the changes in the saturation limits are illustrated in Fig. 4.10.

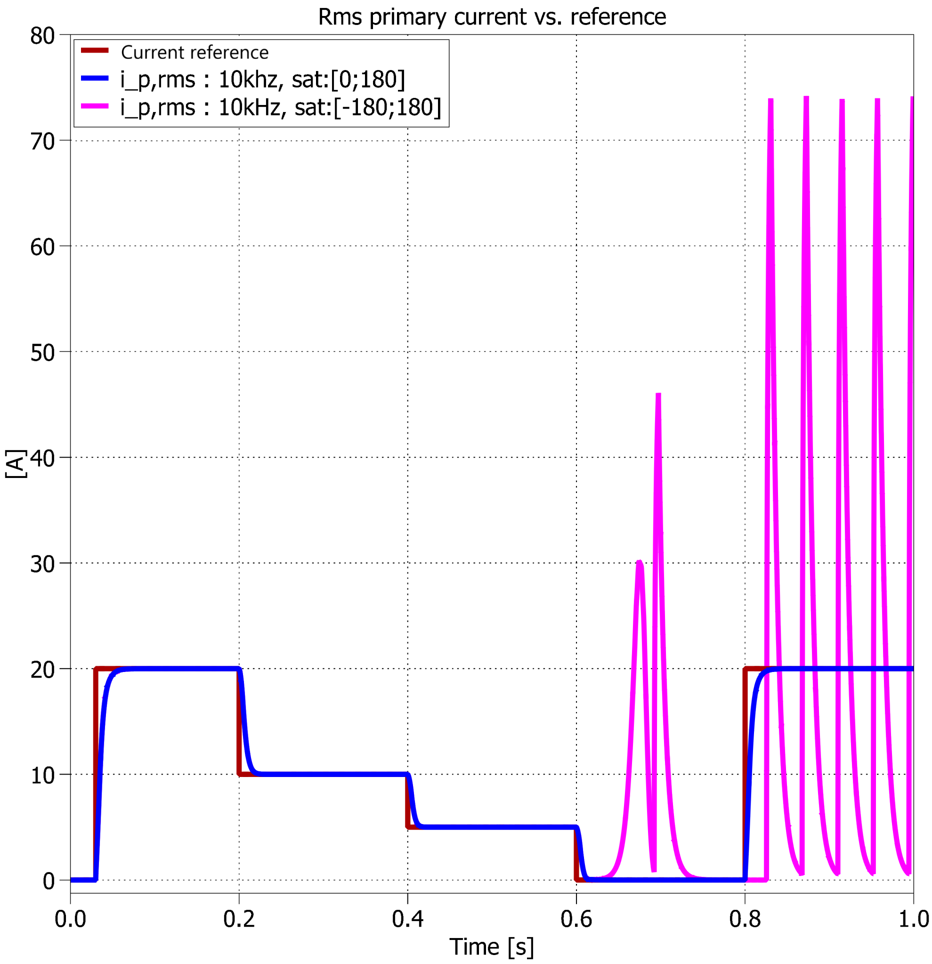

Figure 4.10: Current response with different steps and effect of saturation limit

In Fig. 4.10, the RMS of the measured primary current becomes unstable when the reference is changed to be 0, as seen in the pink measurement. Since the RMS value reaches these high values and is not constant, therefore violates the requirement of a smooth operation. So, the lower limit of the saturation block has been changed, as mention above Fig. 4.10 and illustrated by the blue curve. As shown, the measurement follows the desired reference smoothly and with acceptable speed. The effect of the change in the saturation limits to the controller response is illustrated in Fig. 4.11. Where in Fig. 4.11a, the controller response with the initial saturation limits is illustrated, and in Fig. 4.11b the controller response with the new saturation limits is illustrated.

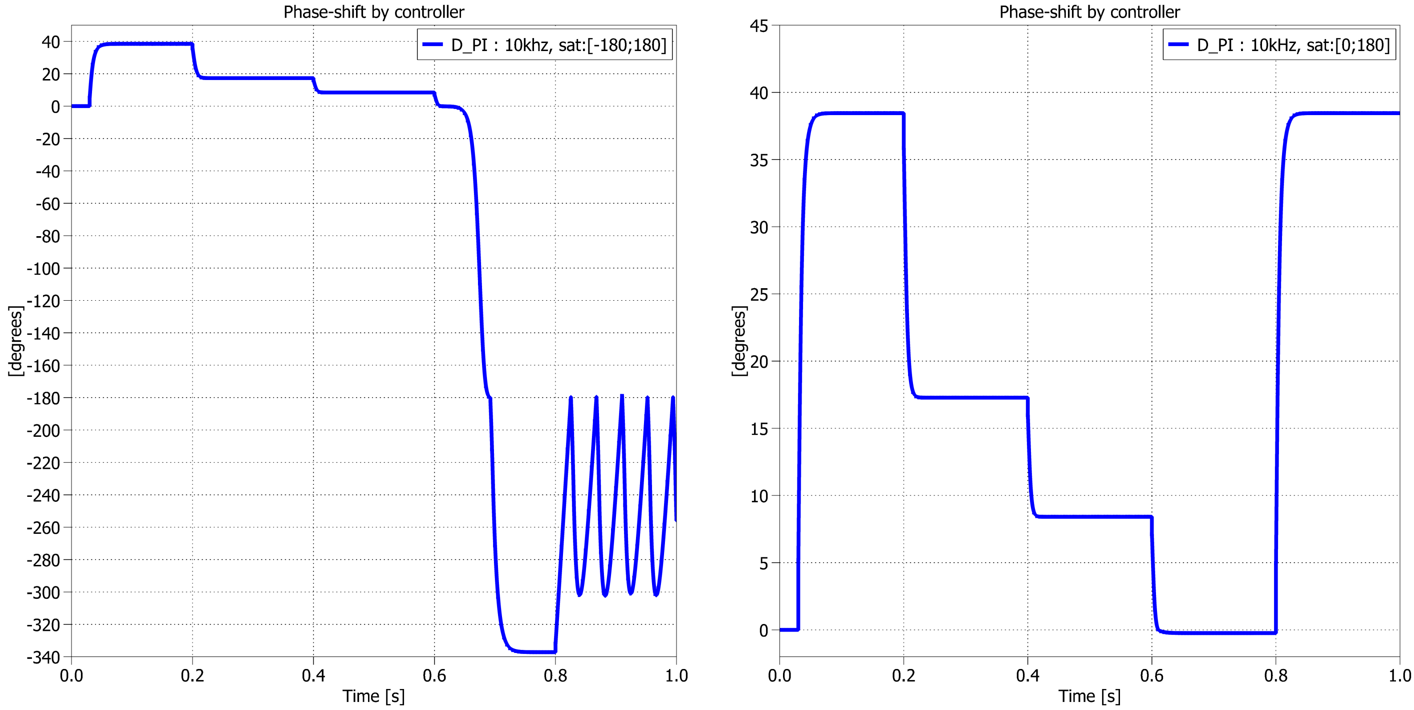

(a) Saturation limit: [-180;180] **(b)** Saturation limit: [0;180]

Figure 4.11: 10 [kHz]: Controller response for reference steps and saturation limit change

The unwanted oscillations in Fig. 4.10 and 4.11 are due to the negative phase-shift of the control. Since the phase-shift influences the power flow through the circulation current path, then a negative phase-shift results in the power being transferred from the primary to the secondary side of the transformer. Thereby, a negative phase-shift removes the power recycling feature of the extended DAB. Therefore the initial saturation limit of $\pm 180^o$ is not intended for this project, where the power recycling is applied. In Fig. 4.11a, when the reference is changed to be 0, the controller output quickly changes to negative values. The phase-shift generated also reaches outside of the saturation limits, and it unable to return to positive values. When the reference is changed back to 20 [A] the controller is unable to return to the range of the saturation block and also oscillates when it reaches the lower limit. On the other hand, in Fig. 4.11b the control smoothly reaches the required phase-shift for each current step. Therefore the smooth and fast operation is achieved.

In order to verify whether the tuned controller is able to function with a new switching frequency, the system is tested with several steps in the current reference and a switching frequency of 250 [kHz].

4.3.2 250 kHz

As the tuned controller from the previous Section is derived with a switching frequency of 10 [kHz], the performance might differ at a different switching frequency. Therefore the performance will be first be tested with a single step change. From Chapter 3 it is illustrated that by increasing the switching frequency, the current amplitude decreases. Therefore to this effect, the current reference of 20 [A] is reduced by a factor of 25 such that the reference becomes 0.8 [A]. By testing the tuned controller with the new switching frequency, the response becomes very slow. This is because the controller is manually tuned to have a smooth response at a switching frequency of 10 [kHz]. Therefore to tune the controller to take into account a change in switching frequency, the PI parameters are dependant on the switching frequency. Therefore the phase-shift controller, expressed in Eq. 4.1, will be changed such that the continuous transfer function becomes as expressed in Eq. 4.2.

$$C_{D,fsw}(s) = K_{p,fsw} + K_{i,fsw} \cdot \frac{1}{s} = \left[0.2 \cdot \frac{f_{sw}}{10 \cdot 10^3}\right] + \left[300 \cdot \frac{f_{sw}}{10 \cdot 10^3}\right] \cdot \frac{1}{s} \tag{4.2}$$

The single-step current responses for the 10 [kHz] tuned and the switching frequency dependant controllers are illustrated in Fig. 4.12.

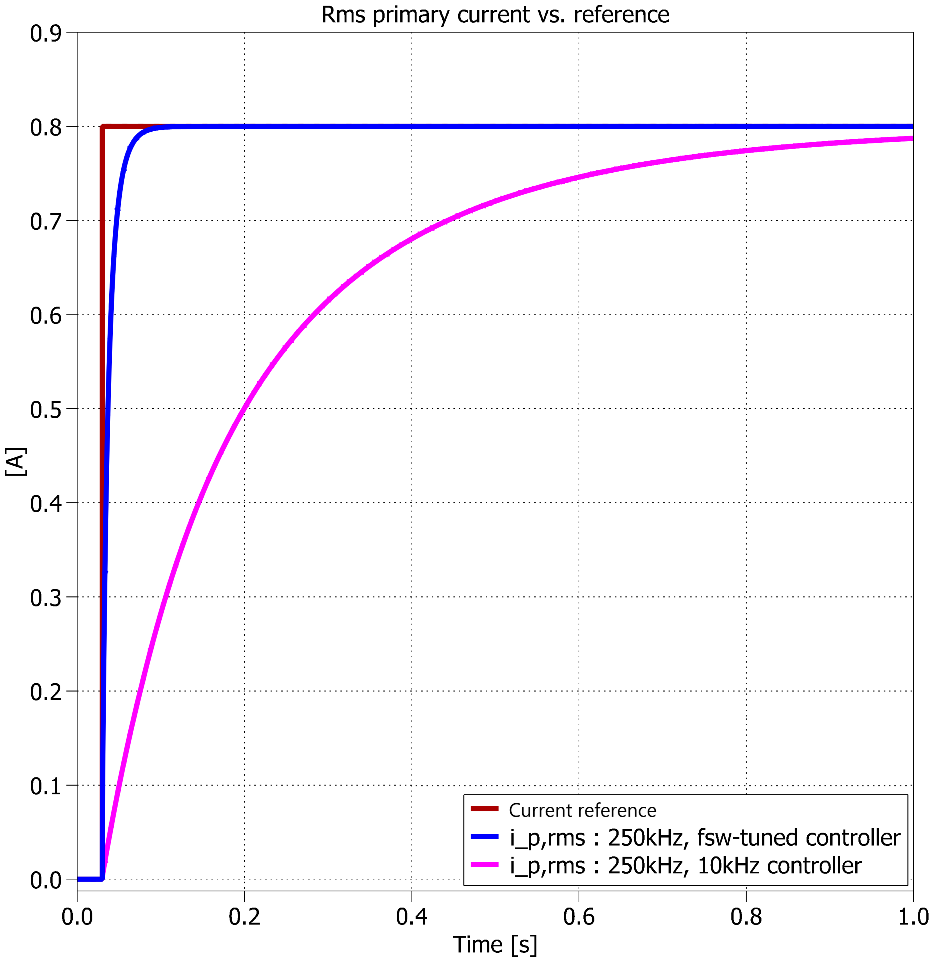

Figure 4.12: 250 [kHz]: Current response with tuned and f_{sw} dependant PI terms controllers

In Fig. 4.12 it can be seen that with the 10 [kHz] tuned controller the current response have greatly been slowed, as previously stated. On the other hand, by changing the PI parameter to be dependant on the switching frequency, the controller has made the response fast with no overshoot and oscillations. Therefore a smooth operation is achieved with the switching frequency dependant PI controller. The controller responses for this single step test are illustrated in Fig. 4.13.

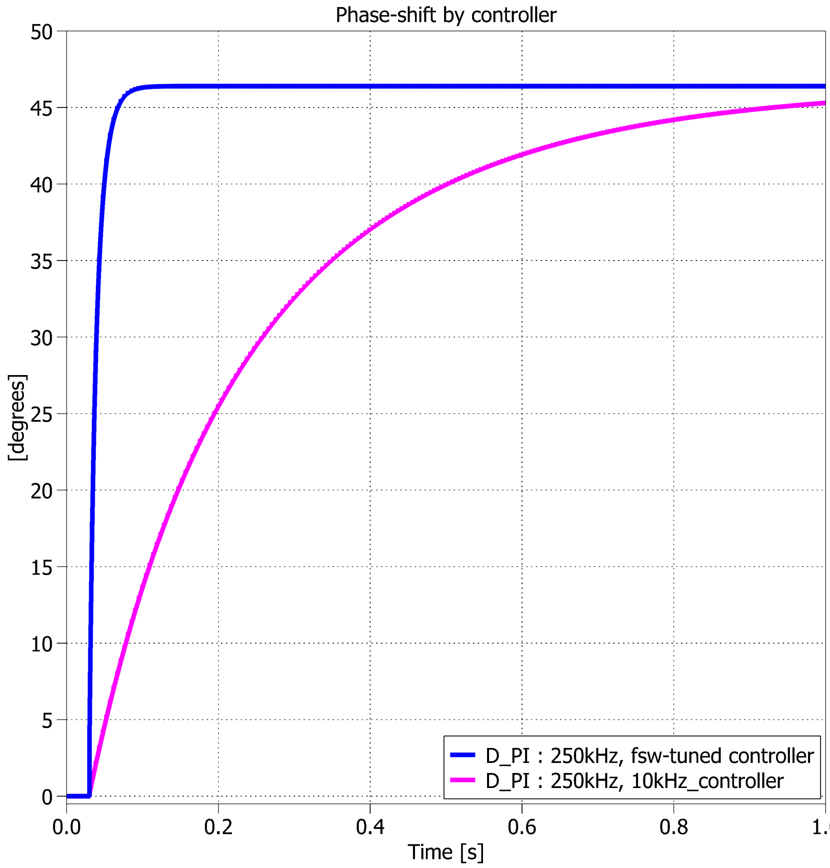

Figure 4.13: 250 [kHz]: Controller response with tuned and f_{sw} dependant PI terms controllers

From Fig. 4.13 the controller responses for the two controllers are illustrated when the switching frequency is 250 [kHz]. The phase-shift reaches the desired value with acceptable speed. From Fig. 4.9 and 4.13, to achieve a RMS current of 0.8 [A] when the switching frequency is 250 [kHz] requires a higher phase-shift, compared to achieve a RMS current of 20 [A] at 10 [kHz]. The maximum current the phase-shift control is able to achieve, and is lower when the switching frequency increases. The phase-shift control is tested with a RMS current reference of 1 [A] and a switching frequency of 250 [kHz], however the control became unstable and reached high negative values. Therefore this reference is ignored and the response is not illustrated.

Since the switching frequency dependant controller functions with a single current step, it is tested with several steps in the reference current. The current steps for this test will follow the same pattern as the 10 [kHz] test, in addition to the same factor reduction as stated at the start of this Subsection. Therefore the current reference for the 250 [kHz] testing is changed in the following order: $0.8 \rightarrow 0.4 \rightarrow 0.2 \rightarrow 0 \rightarrow 0.8$ [A] , where the first value is after the initial step. The current response for this test is illustrated in Fig. 4.14.

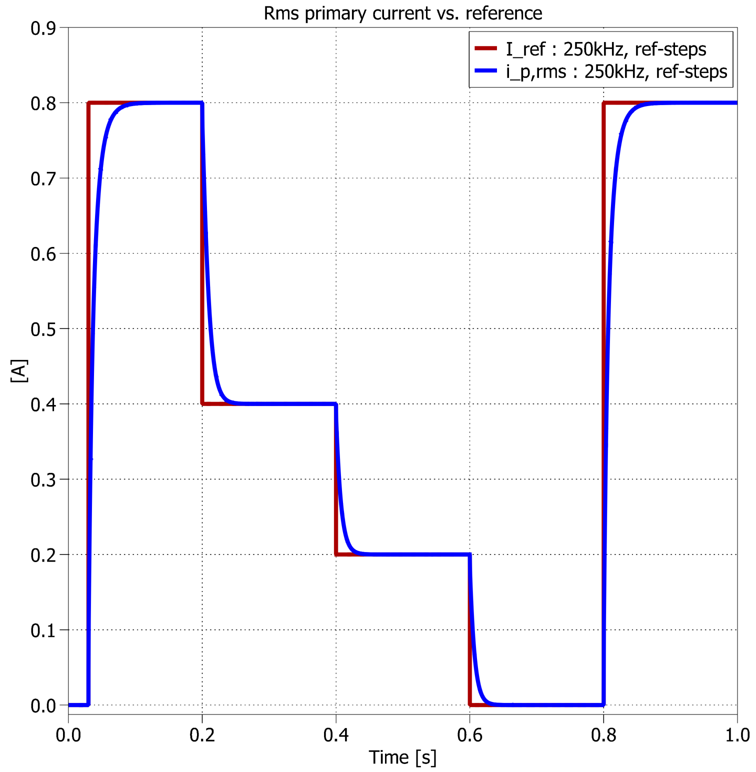

Figure 4.14: 250 [kHz]: Current response with reference steps

In Fig. 4.14, the RMS of the measured primary current smoothly follows the reference. The corresponding controller response is illustrated in Fig. 4.15.

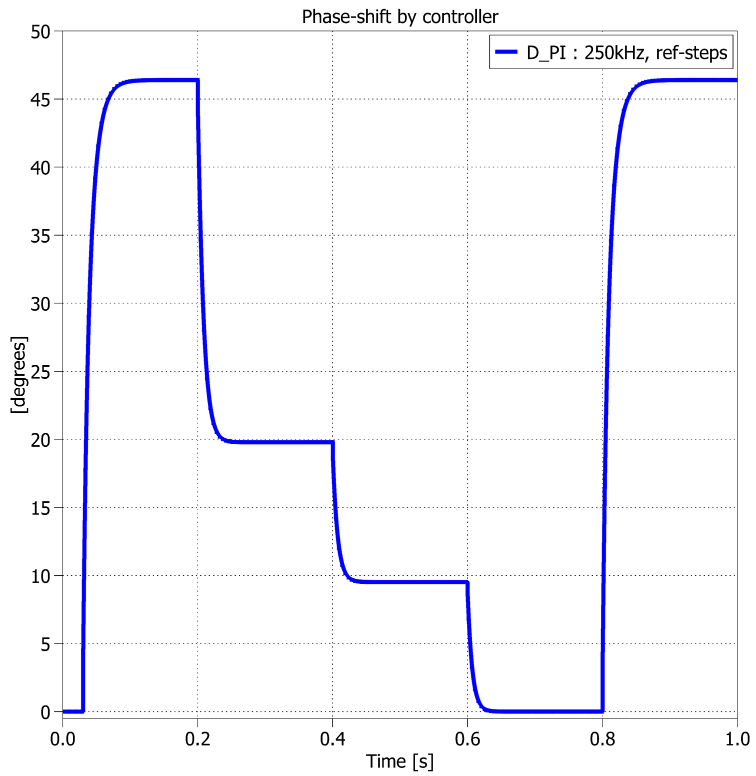

Figure 4.15: 250 [kHz]: Controller response with reference steps

Since the switching frequency dependant PI controller functions with a smooth operation at both extremes of the simulated switching frequency range, the performance of the control in the whole frequency range is assumed to be consistent. The switching frequency dependant controller has been derived with smooth transition between different current values in the simulation, and therefore the next step is to test the performance experimentally.

Chapter 5

Experimental work

In the previous chapter, simulations of the DAB system with a closed-loop phase-shift control is conducted. To validate the control, the DAB system is made in the laboratory and the closed-loop control is implemented and tested. The focus of this chapter is to present the constructed DAB system, the software implementation and test the system control.

5.1 Setup description

Contrary to the simulation system in Fig. 3.1, the experimental setup is with less components. Since the leakage components are a representation of the transformer's primary and secondary side, then these will not be present as they are internal to the transformer. In the Laboratory, minimal voltage is supplied from the DC source instead of the system requirements presented in Table 1.1. It is due to the experimental setup limitation presented in Section 1.6. Therefore, the need for two smoothing capacitors is eliminated. However, to avoid error, a smoothing capacitor will still be present on the input side. Due to the low input voltage supplied, the need for the components such as the resistor, inductor and capacitors on both the primary and secondary side of the transformer shown in Fig. 3.1 are no more required for the experimental setup. Thereby, the experimental setup is minimized to having four passive components. These are the DC source resistor R_{in}, the input dissipation resistor $R_{d,1}$, the output dissipation resistor $R_{d,2}$ and the input smoothing capacitor. The constructed experimental setup is illustrated in Fig. 5.1.

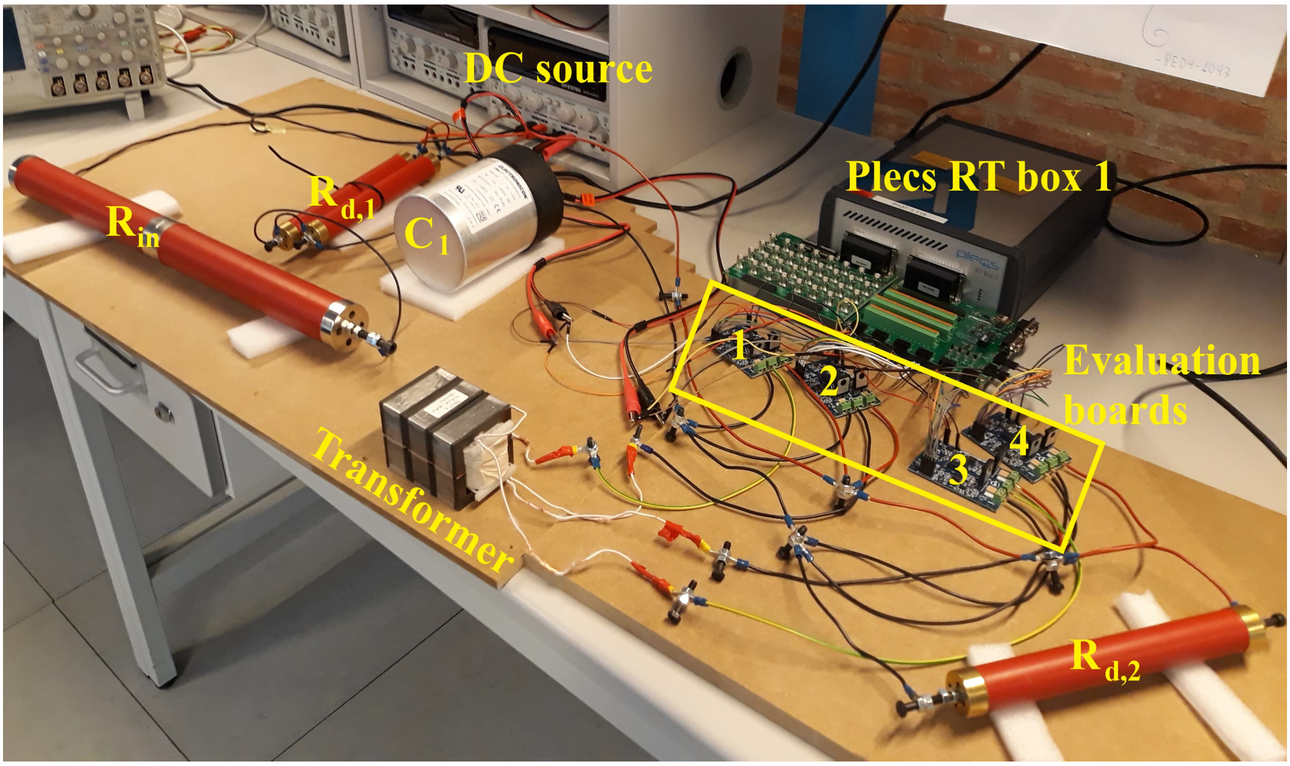

Figure 5.1: Experimental setup circuit diagram

Due to the excess amount of wiring in Fig. 5.1, the connections of the wires are difficult to make out, and therefore, a diagram is made to illustrate the connections. The connections are illustrated in Fig. 5.2. In order to make the connection between the component, the group made use of bolts and nuts, which are illustrated as circles in Fig. 5.2.

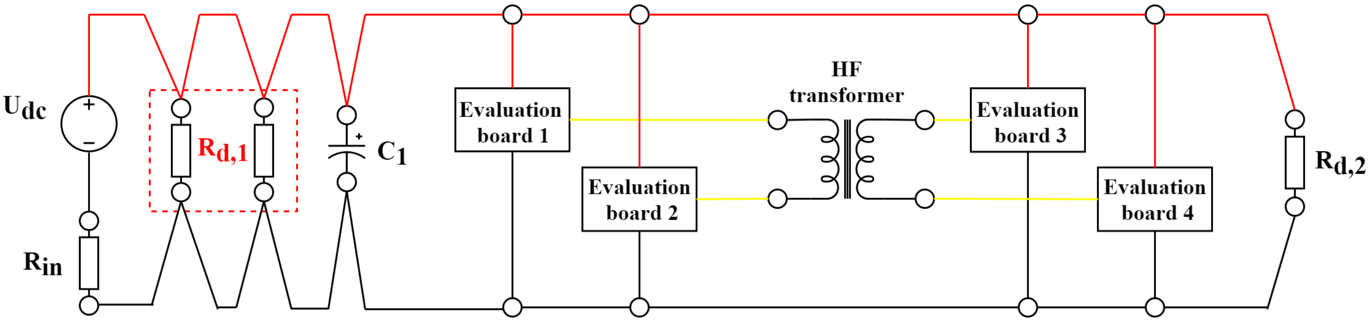

Figure 5.2: Experimental setup circuit diagram

In addition to the wiring illustrated in Fig. 5.2, the wiring from the power supply to the evaluation boards and the connections from the evaluation boards to the PLECS RT box are also present in the experimental setup. The connections from the evaluation boards to the PLECS RT box will be described later in the chapter. The parameters of the four passive components are given in Table 5.1.

Table 5.1: Setup component parameters

Description	Notation	Value	Unit
DC source resistor	R_{in}	4	$[\Omega]$
Input dissipation resistor	$R_{d,1}$	1	$[M\Omega]$
output dissipation resistor	$R_{d,2}$	2	$[M\Omega]$
Input smoothing capacitor	C_1	645	$[\mu\Omega]$

It is noted that the input dissipation resistor is represented by two parallel connected 2 $[M\Omega]$ resistors, as illustrated in Fig. 5.1 and 5.2.

The overall structure is described in this Section, excluding the connections to the PLECS RT box. The function of the PLECS RT box, the connections from the evaluation boards to the PLECS RT box, and the implementations for the PLECS RT box are described in the following Section.

5.2 PLECS RT box

The PLECS RT box is a real-time simulator which has designed specifically for power electronics applications. The RT box is featured with multiple analog and digital input and output channels. In addition, it has Field-Programmable Gate Array (FPGA) embedded CPUs, and therefore, it is a flexible processing unit for both fast control testing and real-time Hardware-in-the-loop (HIL) testing. [14]

For this project, the main task for the RT box is to generate the required PWM signals for the four evaluation boards, and these PWM signals can be generated using the digital channels. The analog channels can be used for voltage and current probes to measure while simulating. In order to control the MOSFETs attached to the evaluation board, it became necessary to configure software for the hardware. Therefore a "PLECS RT box 1" will be applied to the experimental setup. An illustration of the PLECS RT box and the two attached Printed Circuit Board (PCB).

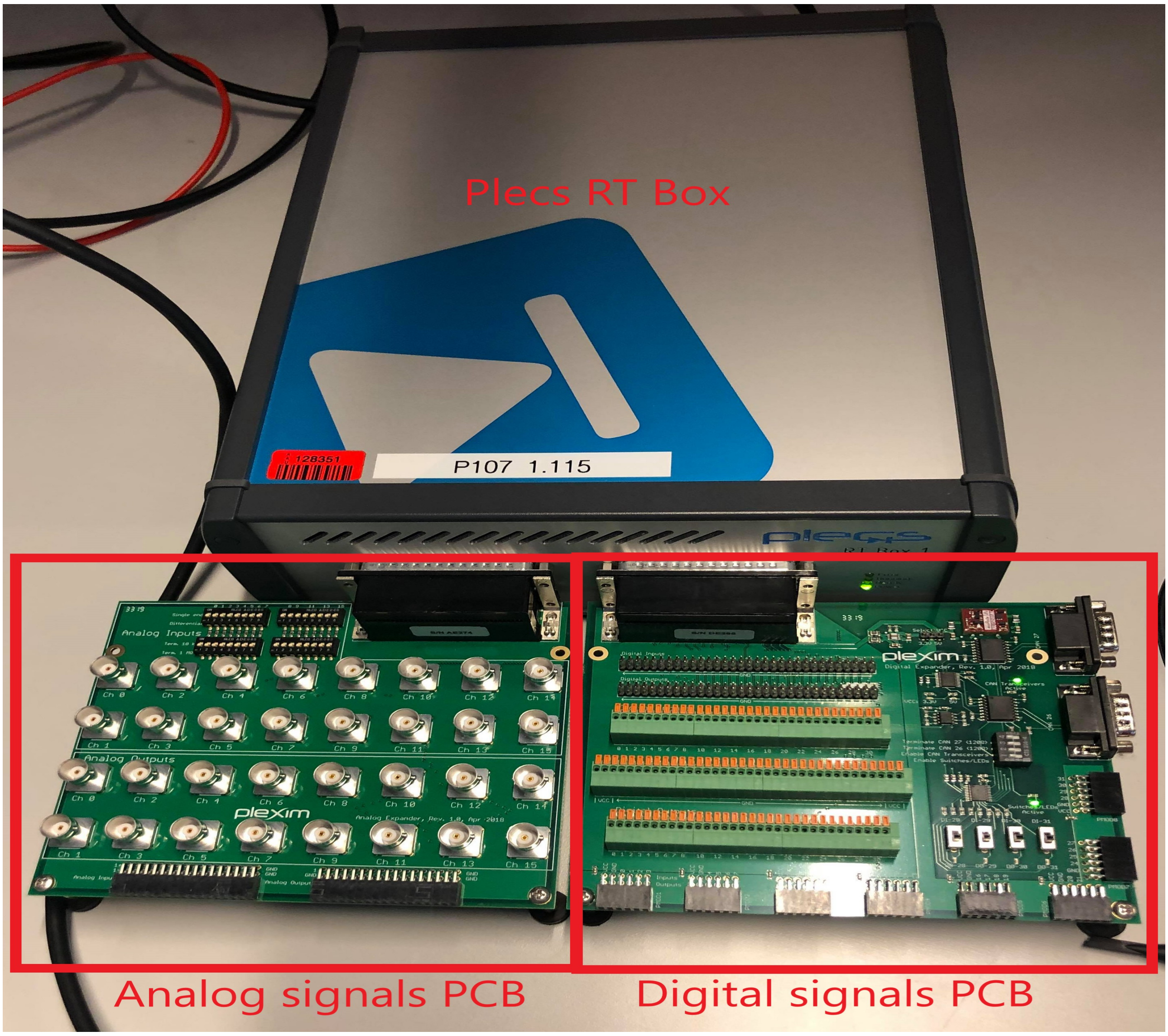

Figure 5.3: PLECS RT box 1 in lab

In Fig. 5.3, the PLECS RT Box is configured with two PCB, such that it is possible to generate both analog and digital signals from the PLECS RT box. By configuring the PLECS RT box, the connections can be defined as either input or output of the box. The digital channels are used to connect the required pins of the evaluation boards, such that needed signals can be defined. To realise the closed-loop control, a feedback of the primary current is required. Thereby the analog PCB is applied to achieve the control.

With the PLECS RT box connected to the evaluation board, the connections of the evaluation board will be described in the following.

5.2.1 Connections

The evaluation board represents a phase leg for the DAB system and therefore four of them are necessary for the system, as illustrated in Fig. 5.1 and 5.2. The evaluation boards used for this project are "*EVAL-1EDI20H12AH-SIC*" [15–17]. A top view of the evaluation board is illustrated in Fig. 5.4.

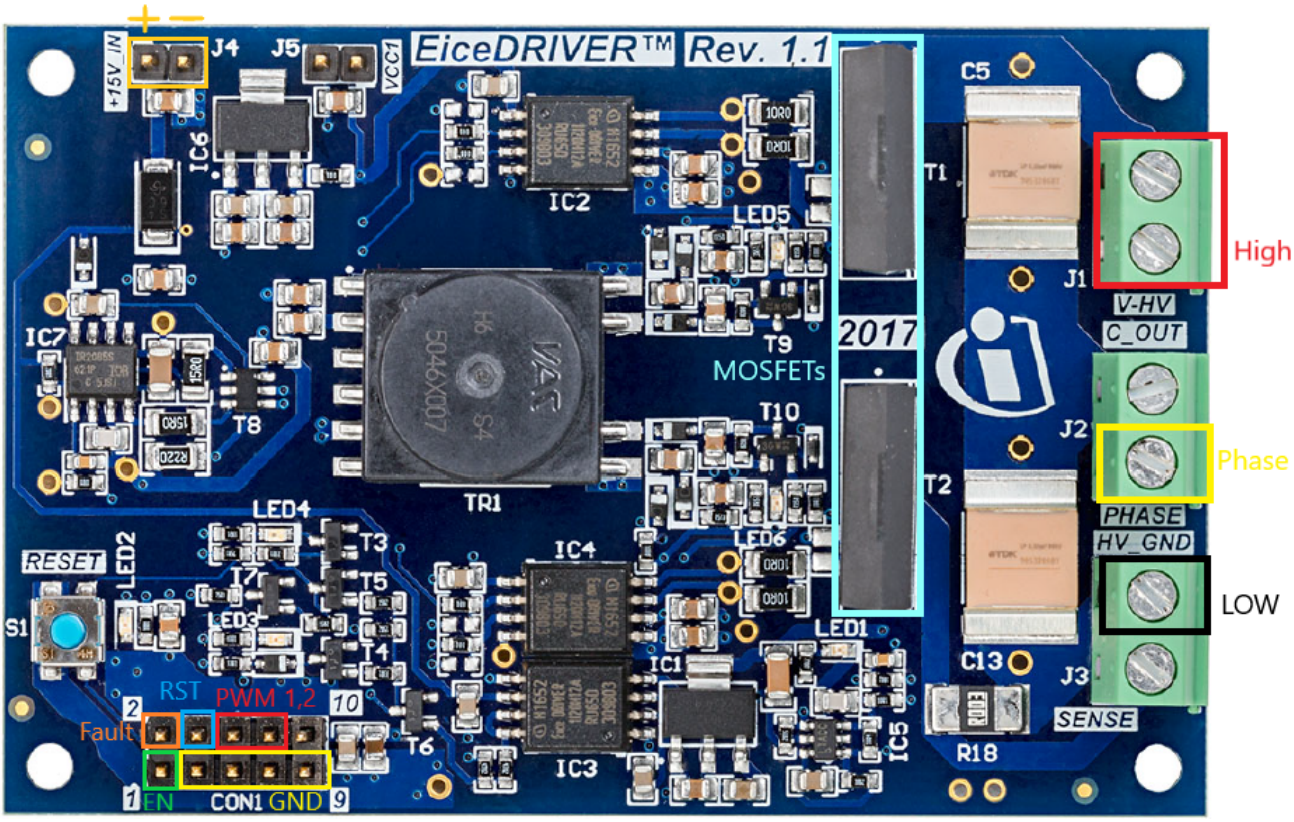

Figure 5.4: EVAL-1EDI20H12AH-SIC top view [16]

In Fig. 5.4, there are four areas of importance. In the top left corner, the evaluation board power supply pins are illustrated. To power the evaluation board, these pins are connected to a 15 [V] DC power supply in the given polarity. In the far right, the circuit connections are illustrated. The "High" and "Low" connections are a representation of the upper and lower point of the half-bridge, respectively. While the "Phase" connection is the wire attached to one of the terminals of the transformer. In Fig. 5.2, these three connections are given for each evaluation board with the same colour notation. Next to the three circuit connection, two MOSFETs of the half-bridge are placed. In the lower-left corner, there are ten pins attached to the board. For this project, only nine of these pins are used. The first pin is the enable pin, denoted as "EN", which allows the half-bridge to switch. This "EN" pin is connected to a digital terminal of the PLECS RT box, and the box defines the input signal for this pin. The second pin is a fault pin, which becomes active when a overcurrent is detected. The "Fault" pin is connected as an input to the RT box such that measures can be performed in case the overcurrent is detected. The third, fifth, seventh and ninth pins are board grounds, denoted "GND", which are connected to the RT box and defined as zero. The fourth pin is a reset pin, denoted "RST", such that the board can be reset in the case of a faulty flip-flop. Like the "Fault" pin, this pin is also connected to the RT box such that measures can be performed. The sixth and eighth pins are the PWM signal pin, where the defined PWM signals from the RT box will be supplied to. Where the sixth pin is for the upper MOSFET in the half-bridge, and the eighth pin is for the lower.

With the description of the evaluation board connection, the implementation of the PLECS modelling to defined the inputs and outputs are described in the following.

5.2.2 Implementations

To get the RT box to function, the RT box is integrated with the PLECS Standalone[13] and the Coder programs[18]. Thereby the PLECS model is translated into a real-time capable C code using the PLECS Coder, which compiles in order to run the RT box. With the feature of being able to connect the original model to the RT box simulation, then RT box measurements can be illustrated and simultaneously able to change the parameters. [14]

In the previous Section, the function of the nine connected pins of each evaluation board to the PLECS RT box is described. In this section, the configuration of these pins in the PLECS modelling for the RT box is described. Each of the used nine pins is connected to the digital PCB. The "EN" pin is defined as an output of the RT box, and therefore, the "Digital Out" block is used for this pin. To make the four evaluation boards be active, the input of the block will be a constant 1, which is applied to the "EN" pin of each evaluation board. All ground pins for each board are connected to an output pin of the digital PCB and are defined in the PLECS Standalone modelling with a "Digital Out" block. As these are grounds, the input of these blocks is a constant zero. For this project, it is only possible to supply minimal voltage, and therefore, the chances of a fault to occur are limited. Therefore each "Fault" and "RST" pin are connected to the RT box, however, protection measures to be defined as future work.

To implement the PWM signals for all eight MOSFETs, there are two methods in the modelling. Either by applying "Pulse Generator" blocks or the built-in "PWM Out"-type blocks can the input of the "PWM" pins be defined. The "PWM Out"-type blocks are a part of the "PLECS RT Box" library for the PLECS Standalone, which is required for the testing. The "Pulse Generator" directly defines the PWM signal to the user specification. The pulses generated by the "Pulse Generator" block will be applied to a "Digital Out" block for the specified pin. On the other hand, the "PWM out" block will output a PWM signal to the specified pin, and its input is the duty cycle of the PWM. The difference between these two PWM methods is that the "PWM Out" a turn-on delay can be defined. Thereby the "PWM Out" is the better alternative for experimental work where dead-time is required, and the duty cycle is close to 50%. However, for the standard "PWM Out" block, the phase-shift is a parameter defined in the interface of the block, and therefore, the closed-loop control derived in Chapter 4 can not be applied to this block. Within the "PLECS RT Box" library, there is an alternative PWM Out block where there are three inputs. Thereby using the "PWM Out (Variable)", it is possible to change the duty cycle, switching frequency and the phase-shift. Therefore the closed-loop control can be realised.

By using the described setup and the "PWM Out (Variable)" block, the testing of the system and the control can be conducted. However, certain limitations are placed upon the project due to COVID-19, stated in Section 1.6. Therefore only the construction of the experimental setup could be performed in the time period of the project, and thereby this will be performed as future work. With this, the experimental setup and work performed in the project time period are described. Therefore the conclusion for this project is derived. The conclusion is given in the following chapter.

Chapter 6

Conclusion

The aim of this project is to design and implement a system that is capable of testing the medium-voltage and high-frequency magnetic component at realistic operating conditions. The exact requirements for the chosen testing system are described in Table 1.1. At first, as per demand of the system, a circuit topology and its operational method is selected based on the literature study. After that, the system is developed and implemented in the PLECS Standalone software in order to get the real-time simulation results. For the detailed analysis of the performance of the system, several tests are performed.

Firstly, in order to analyse the effect of the switching frequency, tests are conducted at different frequency levels. From the results, it is evident that the circulating current is providing current from the secondary side to the primary side of the transformer. Therefore no additional power is supplied from the DC source when higher primary current is present. Additionally, the primary current amplitude is reverse proportional to the increase of the switching frequency. For further analysis, the phase-shift between the gating signals of the converters are varied to different values. The results show that an increase in the phase-shift value resulted in an increase in both the circulating and primary current amplitudes. Additionally, tests are conducted by changing the duty cycle values to obtain its effects on the performance. It is concluded that duty cycle values help to control the power flow in the system. The overall performance from the open-loop testing shows that the system is capable to regulate the power and operate at the desired conditions.

However, the above mentioned open-loop system is not sufficient for practical operations. For the hardware testing, a closed-loop current control system is required. It is also necessary for the robust and smooth operation.

A closed-loop phase-shift controller is therefore designed, implemented and simulated. The details about the designing and implementation of the phase-shift controller are discussed in chapter 4. The controller response for the different K_p and K_i values is also analysed and presented. Using the tuned PI controller, the required phase-shift is generated for the system. For the testing of the closed-loop controller, the current reference is stepped to different values that change after a few hundred milliseconds of time. It is to determine the current response to different current steps. The current steps based reference is tested for the different switching frequencies. From the results, it is clear that the primary RMS current follows the reference current steps accurately, thus validating the system performance.

Furthermore, the performance of the closed-loop controller is aimed to be validated in the hardware setup. For that purpose, the experimental setup, including all the components, is completely built in the laboratory. The parameter details of the experimental setup components are stated in Table 5.1. The PLECS based controller model is introduced to the hardware setup using a PLECS RT box 1. This PLECS RT box 1 is made functional with the help of the PLECS Coder program. The hardware setup is therefore successfully developed, configured and made functional.

However, as mentioned previously, it is not possible to perform the testing on the experiment setup due to the limited time period allowed in the laboratory. Although the system is made functional to conduct different types of testing as performed in chapter 3 and chapter 4, the project time period is not sufficient. Therefore, the hardware testing will be performed as future work.

Finally, from the result analyses, it can be concluded that a realistic magnetic component testing system is developed in this project that is capable of operating at high frequency and fulfilling the project requirements.

Chapter 7

Future work

The purpose of this chapter is to elaborate on several aspects that can be conducted after the allocated time period of this project.

More complex simulations can also be performed in order to determine the performance of the model extensively. It is relevant to perform some simulation tests for the purpose of duty cycle control in Chapter 4. By controlling the duty cycle, the controllability of the testing system can be further investigated.

Model testing for the experimental setup is expected to be performed in the future. Initially, it is the important objective of the project, which is cancelled due to the COVID-19 restrictions. Within the project time period, the wire connections of the experimental setup and the connections from the evaluation boards to the PLECS RT box 1 are established. The configuration of the PLECS RT box 1[14] and the PLECS Coder[18] are made to be functional. Having preliminary connections and functioning of the experimental setup completed, the next step is to perform different tests in order to validate the performance in the laboratory. After the performance validation, the closed-loop phase-shift controller can be applied to the system to enhance the performance. To further validate the performance of the testing system, multiple types of magnetic components can be tested.

Due to the hardware limitations in the laboratory, it is only possible to test the system with a limited voltage level. For future work, testing the system at the required voltage level needs to be performed as stated in Table 1.1.

As stated in Section 1.2, the protection and safety features such as overshoot voltage detection, short circuit detection, temperature control and monitoring etc., are required for practical applications. However, due to the limited time scope of the project, high voltage operations are not considered. Moreover, as discussed earlier, practical testing is not possible to be performed. It is therefore relevant to introduce some protection and safety features for practical operations in future.

The comprehensive analysis of the magnetic field model and design of the transformer can also be an additional work regarding this project. Finite-Element-Method (FEM) is a very effective tool that can be used to determine the magnetic properties of the magnetic components.

Finally, magnetics testing of the system can be performed. While testing the magnetic component, the internal parameters of the component might be influenced during long term testing and/or repetition testing. In addition, for long term testing, the reliability of the magnetic component can be investigated.

Bibliography

[1] S. Ratanapanachote. Applications of an electronic transformer in a power distribution system. PhD thesis, Texas A&M University, 2004. https://core.ac.uk/download/pdf/147124489.pdf.

[2] J.Y. Bian and G.Y. Qiu. The application of power electronic transformer in distribution power system. In Proceedings of the 4th International Conference on Information Technology and Management Innovation, pages 304–310. Atlantis Press, 2015. ISBN 978-94-6252-112-4. https://doi.org/10.2991/icitmi-15.2015.51.

[3] I. Villar. Multiphysical characterization of medium-frequency power electronic transformers. page 234, 2010. http://dx.doi.org/10.5075/epfl-thesis-4622.

[4] H. Y. Lu, J. G. Zhu, and S.Y.R. Hui. Experimental determination of stray capacitances in high frequency transformers. IEEE Transactions on Power Electronics, 18(5):1105–1112, Sep. 2003. ISSN 1941-0107. doi: 10.1109/TPEL.2003.816186.

[5] IWATSU. B-H Analyzer SY-8218 / SY-8219. https://www.iti.iwatsu.co.jp/en/products/sy/sy8218_option_e.html, 2020. Online; accessed 27 May 2021.

[6] M. Mogorovic and D. Dujic. 100 kw, 10 khz medium-frequency transformer design optimization and experimental verification. IEEE Transactions on Power Electronics, 34(2):1696–1708, Feb 2019. ISSN 1941-0107. http://dx.doi.org/10.1109/TPEL.2018.2835564.

[7] Z. Qin, Y. Shen, P. C. Loh, H. Wang, and F. Blaabjerg. A dual active bridge converter with an extended high-efficiency range by dc blocking capacitor voltage control. IEEE Transactions on Power Electronics, 33(7):5949–5966, July 2018. ISSN 1941-0107. http://dx.doi.org/10.1109/TPEL.2017.2746518.

[8] B. Zhao, Q. Song, W. Liu, and Y. Sun. Overview of dual-active-bridge isolated bidirectional dc–dc converter for high-frequency-link power-conversion system. IEEE Transactions on Power Electronics, 29(8):4091–4106, Aug 2014. ISSN 1941-0107. http://dx.doi.org/10.1109/TPEL.2013.2289913.

[9] C. Mi, H. Bai, C. Wang, and S. Gargies. Operation, design and control of dual h-bridge-based isolated bidirectional dc–dc converter. IET Power Electronics, 1:507–517(10), December 2008. ISSN 1755-4535. https://chrismi.sdsu.edu/publications/2008_1_4_IET_PE_DC_DC.pdf.

[10] B. Zhao, Q. Yu, and W. Sun. Extended-phase-shift control of isolated bidirectional dc–dc converter for power distribution in microgrid. IEEE Transactions on Power Electronics, 27(11):4667–4680, Nov 2012. ISSN 1941-0107. https://doi.org/10.1109/TPEL.2011.2180928.

[11] B. Zhao, Q. Song, and W. Liu. Power characterization of isolated bidirectional dual-active-bridge dc–dc converter with dual-phase-shift control. IEEE Transactions on Power Electronics, 27(9):4172–4176, Sep. 2012. ISSN 1941-0107. https://doi.org/10.1109/TPEL.2012.2189586.

[12] K. Wu, C. W. de Silva, and W. G. Dunford. Stability analysis of isolated bidirectional dual active full-bridge dc–dc converter with triple phase-shift control. IEEE Transactions on Power Electronics, 27(4):2007–2017, April 2012. ISSN 1941-0107. https://doi.org/10.1109/TPEL.2011.2167243.

[13] Plexim. Plecs Standalone. https://www.plexim.com/products/plecs/plecs_standalone, 2002. Online; accessed 14 May 2021.

[14] Plexim. RT Box. https://www.plexim.com/products/rt_box, 2002. Online; accessed 12 May 2021.

[15] Infineon Technologies AG. EVAL-1EDC20H12AH-SIC. https://www.infineon.com/cms/en/product/evaluation-boards/eval-1edc20h12ah-sic/, 2017. Online; accessed 12 May 2021.

[16] Infineon Technologies AG. Evaluation Board Manual EVAL-1EDI20H12AH-SIC/EVAL-1EDC20H12AH-SIC. https://www.infineon.com/dgdl/Infineon-Evaluation_Board_EVAL-1EDx20H12AH-SIC-ApplicationNotes-v01_00-EN.pdf?fileId=5546d4625fe3678401601333aa6e192d, 2017. Online; accessed 12 May 2021.

[17] Infineon Technologies AG. Gate-driver Datasheet 1EDIxxI12AH/1EDIxxH12AH. https://www.infineon.com/dgdl/Infineon-1EDIxxy12AH-DataSheet-v02_00-EN.pdf?fileId=5546d46253f6505701543843c049027b, 2016. Online; accessed 12 May 2021.

[18] Plexim. Plecs Coder. https://www.plexim.com/products/plecs/plecs_coder, 2002. Online; accessed 14 May 2021.